Time-dependent wave packet study on trans-cis isomerization of HONO driven by an external field

Falk Richter, Fabien Gatti, Céline Léonard, Frederic Le Quere, Hans-Dieter Meyer

Time-dependent Wavepacket Study on trans-cis Isomerization of HONO with an external field

Falk Richter and Fabien Gatti[*]

CTMM, Institut Charles Gerhardt, UMR 5253,

CC 014, Université Montpellier II,

F - 34095 Montpellier, Cedex 05, France

Céline Léonard and Frédéric Le Quéré[†]

Université de Marne-la-Vallée, Laboratoire de chimie théorique,

EA 2180, 5 boulevard Descartes, Champs-sur-Marne,

77454 Marne-la-Vallée, Cedex 2, France

Hans-Dieter Meyer[‡]

Theoretische Chemie, Universität Heidelberg,

Im Neuenheimer Feld 229, D - 69120 Heidelberg, Germany

(Dated: July 19, 2007)

Abstract

The present paper is devoted to a full quantum mechanical study of the *cis→ trans* isomerization of HONO, similar as in our previous publication (Richter *et al.* [J .Chem. Phys. **120**, 6072 (2004)]). However, the dynamics is now performed in presence of an external time-dependent field in order to be closer to experimental conditions. We show that there is a selective IVR-pathway. *Ab initio* calculations on a six-dimensional dipole moment function are performed. Using the previoulsy developed PES (Richter *et al.* [J .Chem. Phys. **120**, 1306 (2004)]), all eigenstates up to 4000 cm^{-1} are calculated. We simulate the dynamics during and after excitation by a pulse whose parameters are chosen to efficiently trigger the isomerization.

---
[*]E-mail:frichter@univ-montp2.fr,gatti@univ-montp2.fr

[†]E-mail:celine.leonard@univ-mlv.fr,lequere@univ-mlv.fr

[‡]E-mail:hans-dieter.meyer@pci.uni-heidelberg.de

I. INTRODUCTION

Nitrous acid (HONO) is one of the smallest molecules, which exhibits a *cis-trans* conformational equilibrium and the corresponding isomerization presents a strong mode selectivity. Consequently, this molecule constitutes an ideal prototype for theoreticians to investigate the selective intramolecular vibrational-energy redistribution (IVR) leading to a chemical process. Furthemore, since HONO plays an important role in atmospheric chemistry, it has spurred numerous experimental and theoretical works [1–8].

Simulations of the IVR in polyatomic systems are very important since the IVR process can have a decisive influence on the reactivity of the molecular system [9–20]. Much theoretical effort must therefore be directed toward modelling these systems and to further develop general methods of molecular dynamics which, coupled with quantum chemistry calculations, could predict the vibrational states leading to a desired reaction path. In our previous papers [21, 22], time-dependent computations were performed for the *cis-trans* and *trans-cis* isomerizations of HONO. Our calculations confirmed the general trends proposed by classical and quasiclassical trajectory calculations [23–28], i.e. the fact that the *cis-trans* process proceeds much faster than the opposite direction. Moreover, we have shown that there are very large differences between the energy redistributions after different excitations stressing the strong mode selectivity of HONO.

These works can be seen as a part of our studies on IVR in relatively large systems such as a 9 dimensional model of Toluene, [29] Fluoroform [30], HFCO [31], DFCO [32], and H_2CS [33] in their full dimensionality. These investigations aim at developing a systematic study of the IVR for numerous systems and could offer a precious tool for a synergy between experimentalists and theoreticians in this field. Except for H_2CS, the initial excitations were chosen to be excitations of local modes. These preliminary studies were very helpful to highlight the IVR selectivity and the qualitative features of the processes. However, the somewhat artificial excitations of local modes can be very different from excitations which are obtained by irradiation with laser light, the standard way to experimentally excite molecules. In order to truly simulate the dynamics during the interaction with laser pulses, as in the experimental femtochemistry, the next step is then to explicitly implement the

dipole moment surfaces and the external fields in the quantum mechanical simulations. We have already started such a simulation for the H_2CS molecule [33]. This paper aims at going further in this direction and, in particular, at deepening our previous studies on the *cis-trans* isomerization of HONO.

For this, we have calculated an accurate dipole moment function. The dynamics can then be performed, as in our previous articles, by means of the multiconfiguration time-dependent Hatree method [34–37] along with the six-dimensional potential energy surface (PES) calculated in Ref. [21] and the exact kinetic energy operator in polyspherical coordinates provided in Ref. [22]. It is then possible to find efficient pathways leading to the isomerization and tailored femtosecond laser pulses which can trigger this reaction. The outline of this study is as follows. In Section II, we explain the theoretical model which constitutes the framework of our simulations and bring out a selective pathway leading to the isomerization. Section III is devoted to the presentation of the new six-dimensional dipole moment function. After a brief presentation of MCTDH in section IV, the vibrational levels up to 4000 cm^{-1} and the corresponding transition moments are given in section V. Finally, section VI displays the dynamics with the chosen parameters of the pulse and the paper draws perspectives for the future.

II. TOWARDS A MODE SELECTIVE *CIS-TRANS* ISOMERISATION

A. Model

In reference [22], the dynamics was performed with a time-independent hamiltonain operator :

$$\hat{H}_0 = \hat{T} + \hat{V} \tag{1}$$

where $\hat{T}$ is the exact kinetic energy operator for total $J = 0$ and in terms of the six valence polyspherical coordinates given in the Appendix of Ref. [22]. $\hat{V}$ is the six dimensional potential energy surface calculated in Ref. [21] and expressed in terms of the same coordinates.

To explicitely include a laser pulse in the dynamics, the system will be described by a time-dependent Hamiltonian :

$$\hat{H}_{tot} = \hat{H}_0 + \hat{h}(t) \tag{2}$$

where, $\hat{h}(t)$ represents the first order interaction of the molecule with a classical external laser field $E(t)$ [38], i.e.

$$\hat{h}(t) = -\hat{\vec{\mu}} \cdot \vec{E}(t), \tag{3}$$

where $\hat{\vec{\mu}}$ is the Dipole Moment operator. We have neglected the effect of polarisability in this equation, however, we will estimate its influence in Section III. In order to mimic a laser pulse, we adpot the following form for the external field:

$$\vec{E}(t) = E_0 \, cos(\omega t) \, sin^2(\pi t/t_p) \, \Theta(t) \, \Theta(t - t_p) \, \vec{e} \tag{4}$$

where E_0 is the field strenth, ω the field frequency, $\Theta(t)$ the Heavyside's step function, t_p the pulse duration and $\vec{e}$, the unit vector in polarization direction.

In our model, we assume the molecule being "ideally oriented" [39], i.e. a molecule where the Euler angles of the Eckart frame $\alpha_E, \beta_E, \gamma_E$ are fixed (rigid constraints: $\dot{\alpha}_E = 0, \dot{\beta}_E = 0, \dot{\gamma}_E = 0$, here $\dot{q}$ denotes $\frac{dq}{dt}$). Molecular orientation is a current active research field [40–45]. Polar molecules can be indeed (partially) oriented in the gas phase by a static field ("brute force method" [40]) or by an external field which varies smoothly

4

in a way that it is concerted with the internal motion [46].

We have to note that the kinetic energy operator which we are using (eq. (1)) does not describe such an oriented molecule (which corresponds to a superposition of an infinite number of J states), but a J=0 situation, i.e. equivalent to $\frac{d}{d\alpha_E} = 0, \frac{d}{d\beta_E} = 0, \frac{d}{d\gamma_E} = 0$. However, we shall keep the J=0 operator since its expression is far more simple. Generally, the two situations (J=0 and oriented molecule) lead to two different kinetic energy operators [47]. This point has been indeed adressed in reference [48] (reviewed in Ref. [49, 50]), in which the rigorous derivation of rigidly constrained kinetic energy operators was presented in a full *ab initio* and general context. Such constrained expressions were applied several times (see for instance [50]) and experience shows that the correction term obtained by properly imposing $\dot{q} = 0$ compared to simply putting $\frac{d}{dq}$ to zero results in often numerically small corrections which are important only in accurate infrared spectroscopy (see [51] for an application for which such corrections are included).

Hence, our model assumption is, that the Eckart frame [52] (in which the rotation of the molecule is zero by definition) keeps an initially choosen spatial orientation throughout the excitation process. Consequently, the dipole vector depending on the Euler angles will be refered to the Eckart axis system and the laser field can be oriented parallel to an axis of choice. Marquardt and coworkers [39, 53, 54] have already extensively discussed this model of the "ideally oriented" molecule. In particular, they have investigated a diatomic system coupled with a laser field (time-dependent). The authors oriented the molecule with the aid of a second field (static). Therein, it was shown that the vibrational dynamics of the complete treatment (including the rotation) converges to the dynamics of the 'pure vibrational model' (J=0) as in eq. (2) at reasonable field strengh. Consequently, it is very reasonable to think that the dynamics is not very different when considering an hamiltonian operator for which the molecule is oriented or when taking the J=0 case as in eq. (2).

B. A mechanism for selective isomerization.

In order to trigger the process by means of a laser field, a dipole moment function is needed and a proper choice of the maximum field strength, the frequency and the pulse duration of the laser excitation (eq. (4)) has to be made. In this work, we decided to focus on excitations which lead to a final energy of about 1. eV above the minimum of the PES (the zero-point energy corresponds to about 0.45 eV of vibrational excitation energy). We did so for two reasons: first, for comparing our results with our previous ones [22]. Secondly, because the quality of our PES (ref. [21]) is not assured higher in energy.

Since the $cis \rightarrow trans$ isomerization is much faster than its opposite, we will focus on the cis geometry in this paper. (The true ground state is in trans geometry). In particular, we will start the dynamics from the ground state in this geometry.

Moreover, in Ref. [22], we have shown that the most efficient local modes for triggering the $cis \rightarrow trans$ isomerization are the ON middle stretching and the HON bending modes. For all propagations, we artificially excited local overtones such that the total energy was close to about 1. eV. About 12 percent was isomerized after 2 ps for both cases. While the excited HON bending mode tends to rapidly distribute the energy among all the modes, the energy after ON stretching mode excitation mostly remained localised in the ONO/ON modes (see Figures 2 and 3 in Ref. [22]). Following the analysis in [21], the isomerization after ON stretching mode excitation is essentially driven by an efficient potential coupling with the torsional angle. It was indeed shown (Fig. 4(b) in Ref. [21]) that the barrier height is considerably lowered when the ON stretching mode is allowed to adjust. On the contrary, numerous complex resonances with all the modes of vibration can explain the energy transfer into the torsional mode in the case of HON bending mode. Since we are interested in a *selective* isomerization proccess, we will thus focus on the ON excitation only and exclude as much as possible the HON bending mode excitation which leads to a statistical energy distribution, i.e. to a non-selective IVR. Consequently, it is intuitive to think that an external field parallel to the ON bond, i.e. to the z^{BF} axis is a good starting choice.

In the following, we present in more details the essential properties of the PES which might account for an efficient isomerization and then propose an excitation exploiting these potential features.

The six internal (valence) polyspherical coordinates describing the systems are depicted in Figure 1. First of all, it must be pointed out that it is little probable that the isomerization follows the minimal energy path if the torsion is not directly excited. Indeed, this minimal energy path mainly involves the torsion (see Ref. [21]). Moreover, the barrier height is about $4000\ cm^{-1}$ above the *cis* minimum while the ground state energy of the torsion alone can be estimated to be about $300\ cm^{-1}$ (in a good approximation, since the torsion is weekly coupled with the other modes for the ground-state). If one (non-torsional) mode is excited, we can estimate that the energy transfer into the torsional mode will not exceed $1000\ cm^{-1}$, if the total energy remains below 1. eV. Therefore, we are looking for an isomerization path, which might have an absolute barrier higher than the minimal energy path, but whose 'potential barrier' B_τ defined as

$$B_\tau = V(R_1, R_2, R_3, \theta_1, \theta_2, \tau_{top}) - V(R_1, R_2, R_3, \theta_1, \theta_2, \tau = 0) \qquad (5)$$

can be much smaller than the barrier height of the minimal energy path. In eq. (5), V is the HONO potential and $\tau_{top} = \tau_{top}(R_1, R_2, R_3, \theta_1, \theta_2)$ is the value of the torsional angle which maximizes V for fixed values of $R_1, R_2, R_3, \theta_1, \theta_2$. $B_\tau(R_1, R_2, R_3, \theta_1, \theta_2)$ can then be interpreted as the barrier height to proceed the isomerization from *cis* to *trans* by changing only the torsional coordinate at a given value for the other coordinates. In the limits $R_1 = \infty$, $R_2 = \infty$, $R_3 = \infty$, $\theta_1 = 180°$ or $\theta_2 = 180°$ B_τ will tend to zero. A systematic study of B_τ (not explicitly presented here) shows the following properties. In the considered energy regime, the ON stretching mode - as expected - but also the ONO bending mode, have significant influence on B_τ. While variations of only ONO hardly influence this barrier height, a combined variation of ON and ONO does. The other coordinates have negligible influence on B_τ. More important, a simultanious elongation of R_3 and an increase of $cos(\theta_2)$ diminishes B_τ effectively. To provide an estimate, B_τ reaches the value of about $1000\ cm^{-1}$ at about $R_3 = 3.0$ bohr and $cos(\theta_2) = -0.25$. For comparison we recall that the equilibrium

values are $R_3 = 2.7$ bohr, $cos(\theta_2) = -0.35$ and $B_\tau = 4700$ cm^{-1}. As shown later, the former values correspond to meanvalues which can be attained during a propagation with 1 eV total energy. For higher values of R_3 and $cos(\theta_2)$, B_τ falls very quickly to less than 500 cm^{-1} within the grid ranges considered in this work.

The desired excitation should minimise B_τ with a minimal effort. Therefore, we define a geometry '$(R_1^{opt}, R_2^{opt}, R_3^{opt}, cos(\theta_1^{opt}), cos(\theta_2^{opt}))$' as belonging to the optimal path if this geometry minimizes B_τ with respect to all the geometries which are isoenergetic. Of course, the optimal path does not necessarily have to coincide exactly with the steepest descent path suggested by $B_\tau(R_3, cos(\theta_2))$. However, we have observed that the optimal path deviates only slightly from the latter within the considered energy range. Other coordinates than R_3 and $cos(\theta_2)$ do not undergo considerable change along the optimal path. The optimal path is depicted in the Figure 2 (thick broken lines) overlayed with chosen cis eigenfunctions strongly located along the optimal path. (Note that this figure will be discussed in more detail in section VI.) We can already conclude from figure 2, that efficient isomerization is expected when a wave packet motion is induced introducing a simultaneous increase of R_3 and $cos(\theta_2)$. Consequently, in the analysis of the eigenstates in section V, we will focus on those eigenstates in the *cis* geometry which can compose such a motion.

FIGURE 2 AROUND HERE

8

III. DIPOLE MOMENT SURFACE

The six-dimensional Dipole Moment Surface (DMS) was generated by *ab initio* calculations using the density functional theory aproach with the B97-1 functional [55] implemented in CADPAC [56]. The TZ2P basis set (ref. [57] and references therein) was employed. It is known from various calculations [21] that the electronic wavefunction has only one dominant determinant for the considered geometries. 924 dipole moment vectors were calculated by DFT for geometries in the region $1.3 < R_1 < 2.6$ bohr, $1.8 < R_2 < 2.7$ bohr, $2.0 < R_3 < 3.85$ bohr, $170° < \theta_1 < 100°$, $170° < \theta_2 < 50°$, and $-90° < \tau < 90°$. The molecular body-fixed system is centered at the O central atom, the z axis points along O$\rightarrow$N, and its zx plane is in the ONO plane, such that the terminal O atom lies in the (xz, x $>$0) half plane. The dipole moment vectors were calculated starting from the body fixed frame as a space fixed frame and then rotated to the Eckart frame [52]. The x component of the Eckart transformed dipole moment vector has been fitted to the following form:

$$\mu_x(R_1, R_2, R_3, \theta_1, \theta_2, \tau) = \sum_{ijklmn} c^x_{ijklmn} R_1^i R_2^j R_3^k \theta_1^l \theta_2^m \cos(n\tau) \tag{6}$$

Using finally the restriction:

$$i + j + k + l + m + n \leq 4; \tag{7}$$

$$\tag{8}$$

the 210 coefficients (available upon request) were calculated using a least mean square procedure. For the z-component $\tanh(0.7(R_3 - 2.2))$ was choosen instead of R_3 as fit coordinate in order to describe a turning point of μ_z appearing along the R_3-stretch. The parameters appearing in the tanh were optimised. This modification lowered the root mean square error by about a factor of $1/2$. For the y-component $\sin(n\tau)$ was used as the fit function for the torsion and n was additionally restricted to $n > 1$ to adopt the odd symmetry for this case resulting in 86 terms only. The root mean squares of the fits were about 0.0014, 0.0002, 0.0020 a.u. for the x, y, z components, respectively. The convergence of the fit can be estimated by comparing the variationally averaged dipole moments and the transition moments resulting from the described surfaces with those obtained from surfaces fitted with about twice the number of terms.

Finally we have estimated the influence of the polarisability α on the dynamics using the following ratio :

$$\left| \frac{1/2\alpha_{zz}^{eq} E_o^2}{\mu_z^{eq} E_o + 1/2\alpha_{zz}^{eq} E_o^2} \right| \tag{9}$$

where α_{zz}^{eq} and μ_z^{eq} denote the polarisability and the dipole moment respectively calculated at the equilibrium geometry. For an external field whose intensity is equal to 0.003 a.u., the effect of the z-component of the polarisability is equal to about 12 % of the value of the effect of the z-component of the dipole moment. In this paper, we will thus neglect the contribution of the polarisability, $1/2\vec{E}^T(t)\alpha\vec{E}$, in the time dependent operator $\hat{h}(t)$ (eq. (3)).

IV. MULTICONFIGURATION TIME-DEPENDENT HARTREE

All the dynamical calculations discussed in this article are performed with the multiconfiguration time-dependent Hartree (MCTDH) method, which is a powerful method for propagating multidimensional wave packets. We have used the Heidelberg MCTDH package [58], which is a set of programs for propagating, analyzing and visualizing wave packets.

As MCTDH is well documented in the literature [33–37], we do not discuss it here in detail. However, we want to emphasize that – due to a recent development – MCTDH cannot only solve the time-dependent Schrödinger equation but the time-independent one as well. Eigenstates and their energies may be calculated by the so called *improved relaxation* algorithm [33, 37].

Turning to the calculations discussed below we note that the same mode-combination scheme is used as in our previous publication [22], i. e. $[R_1, \tau]$, $[R_3, \theta_2]$ and $[R_2, \theta_1]$. The primitive grids used are similar to Ref. [22].

V.   VIBRATIONAL EIGENFUNCTIONS AND INTENSITIES OF *cis*-HONO

The harmonic frequencies ω_i of the different vibrational modes for the *cis* geometry are given in Table I. The (anharmonic) fundamentals ν_i are also given in Table I and compared with experimental values.

<center>TABLE I AROUND HERE</center>

In order to obtain the eigenstates, the previously developed *improved Relaxation* method [33, 37] was employed. For the convergence of the desired eigenstate with this method the choice of the initial guess is crucial. The user has indeed to define an initial state which should have a decent overlap with the eigenstate one wants to compute. In this paper, we decided to generate the initial guess by single harmonic excitations of already calculated eigenfunctions. This single harmonic excitation was obtained by applying the corresponding raising operator to the lower eigenfunction which is the closest to the sought state. For example, the initial guess for an eigenfunction which could be tentativaly assigned as, say 012340 , would be $a_5^\dagger$012330, $a_5^\dagger$ beeing the raising operator for mode 5 and 012330 a previously converged eigenfunction tentativaly assigned as 012330. This procedure was robust enough to deal with the various resonances appearing in HONO. In particular, this procedure is far more efficient than choosing the harmonic eigenfunctions as initial states.

Indeed, we have found that the squared overlap between the initial guess and the final wavefunction was often considerably larger than the squared overlap between the harmonic eigenstate and the final wavefunction (see Table 2). (The harmonic eigenstates were obtained by converging the ground state of the harmonic hamiltonian and by applying the various raising operators to it). It should be emphasized that the aformentioned raising operators are not the raising operators in terms of the (usual) rectilinear normal coordinates. The former are defined as:

$$a_\alpha^\dagger = \frac{1}{\sqrt{2}}(Q_\alpha + \hbar\frac{\partial}{\partial Q_\alpha}) \tag{10}$$

with Q_α beeing the *curvilinear* normal coordinate associated with mode α. We define *curvilinear* normal modes as in Ref. [31], i.e. starting from a zero order harmonic Hamilto-

<center>12</center>

nian $\hat{H}^o$ expressed as

$$\hat{H}^o = \frac{1}{2} \sum_{n,m=1}^{6} (q_n - q_n^{eq}) F_{nm}(q_m - q_m^{eq}) + \hat{p}_n G_{nm}^o \hat{p}_m , \qquad (11)$$

where $\hat{p}_n = \partial/\partial q_n$, $\mathbf{G^o}$ represents the functions appearing in the kinetic energy operator (eq. (A2) in ref. [22]) fixed to their values at the equilibrium geometry $\mathbf{q}_{eq}$, q_n and q_m denote the 6 polyspherical coordinates and the $\mathbf{F}$ matrix corresponds to the harmonic approximation of the potential: $F_{nm} = \partial^2 V/\partial q_n \partial q_m|_{\mathbf{q}_{eq}}$. In order to define *curvilinear* normal modes $\{Q_\alpha\}$ in terms of the polyspherical coordinates, one diagonalizes the matrix $\mathbf{F\,G^o}$ such as

$$\mathbf{F\,G^o\,L} = \mathbf{L}\,\omega^2 \qquad (12)$$

where ω^2 denotes the diagonal eigenvalue matrix and $\mathbf{L}$ is the eigenvector matrix. The *curvilinear* normal coordinates Q_α are related to the polyspherical coordinates as

$$Q_\alpha = \omega_\alpha^{1/2} \sum_{n=1}^{3N-6} (q_n - q_n^{eq}) L_{n\alpha} . \qquad (13)$$

Let us return to the PES. The spectral properties resulting from the present PES have been already presented elsewhere [21]. In Ref. [21], the vibrational energy levels have been calculated variationally using a method developed by Carter and Handy [59] and a slightly modified PES. Tables II, III and IV compare the latter results with the *cis* vibrational energy levels obtained in this work using the improved relaxation method and the *unmodified* PES.

TABLE II AROUND HERE

TABLE III AROUND HERE

TABLE IV AROUND HERE

In the energy range up to 2500 cm^{-1} the variational levels were expected to have been converged to within 1 cm^{-1} in Ref. [21]. In Ref. [21] the PES was slightly adjusted in order to bring the *cis*-ν_1 level closer to the corresponding experimental value. This lowered the ν_1 value by about 10 cm^{-1} and the remaining variational levels by less than 1 cm^{-1}. When computing the levels with improved relaxation we learned that this artificial modification

of the PES was unnecessary. The too high cis-ν_1 level was due to a lack of convergence and not due to an error in the surface. This problem can be traced back to the contraction scheme which is utilized in the variational code. This contraction scheme indeed optimizes the basis functions with respect to one geometry only associated with one of the two wells (to be precise, we took the *trans*-well). The whole Hamiltonian is then diagonalised in this precontracted basis set. Consequently, this contraction scheme can not be very efficient for both wells together. On the contrary, the MCTDH results are reliable even for these difficult cases. Indeed, they do not depend upon such a rather unflexible contraction scheme, for, in principle, MCTDH probes the whole primitive space to find an optimal solution. The artificial modification of the PES was hence removed. This explains why the variational levels up to about 1000 cm^{-1} are slightly lower in energy with respect to MCTDH results which are the more accurate ones. Otherwise (below 2500 cm^{-1}), the variational energy levels are slightly higher by up to about 1 cm^{-1} compared to the MCTDH ones. There are significant exceptions to this trend, for instance the levels including excitations of the N=O stretch. In particular, the N=O fundamental level at 1632 cm^{-1} is about 8 cm^{-1} lower than the variationally calculated value. The fundamental levels of the unmodified PES are still in excellent agreement with the experimental values although *cis* ν_2 lies now -9 cm^{-1} off the experimental value. This discrepency is not surprising. In the literature it is stressed several times that also CCSD(T) level calculations underestimates the anharmonic N=O stretching in HONO (for instance p. 8803 in [60]). On the other hand, it should be added that due to the use of a large basis set in the CCSD(T) calculations (cc-pVQZ spdf) this error is as low as -9 cm^{-1}. In the energy regime higher than 2500 cm^{-1} - excluding the OH stretch fundamental level - the MCTDH results are lower than the variational ones in energy up to about 20 cm^{-1}, as expected.

The squared overlaps, c_{harm}^2, of the eigenfunctions with the corresponding eigenfunctions of the "harmonic" Hamiltonian are given in Tables II, III and IV. Interestingly enough, these values are usually smaller than 0.5, even for some of the fundamental levels. Even the ground state appears to be strongly correlated underlining the strong anharmonicity of the potential. However, these small values of c_{harm}^2 can also be traced back to the various resonances appearing in *cis*-HONO. As shown in Ref. [21], the eigenfunctions of the one dimensional ON and ONO modes are nearly degenerate and there is therefore a strong

14

coupling between these two modes. This is why the corresponding eigenfunctions (0000a0 and 000a00) are mainly composed of the symmetric and antisymmetric superpositions of the corresponding local modes. The symmetric and the antisymmmetric directions are here thought to be along the $Q^+_{ONO/ON}$ and $Q^-_{ONO/ON}$ axes, respectively, defined as $Q^\pm_{ONO/ON} = (R_3 - R_3^0) \pm (\cos(\theta_2) - \cos(\theta_2^0))$. The small c^2_{harm} values for 000010 and 000100 arise from the fact that the antisymetric superposition (located along the $Q^-_{ONO/ON}$ axis) refers to 000010 (616 cm^{-1}) and the symmetric one (located along the $Q^+_{ONO/ON}$ axis) refers to 000100 (850 cm^{-1}) while the contrary is true for the harmonic eigenfunctions $(000010)_{harm}$ (644 cm^{-1}) and $(000100)_{harm}$ (882 cm^{-1}). It is not surprising that small perturbations can lead to drastic changes in the wavefunction when resonant cases are considered. Indeed, while the harmonic potential in the $Q^-_{ONO/ON}$ direction is slightly weaker than in the $Q^+_{ONO/ON}$ direction, inclusion of anharmonic potential terms slightly distorts the potential such that $Q^+_{ONO/ON}$ is now the weaker one and the symmetric superposition becomes the lower solution of the resonant pair. In section II B, it was shown that an efficient isomerization is expected when a wave packet motion is induced by a simultaneous increase of R_3 and $cos(\theta_2)$. This motion corresponds to the excitation in the $Q^+_{ONO/ON}$ direction. This is why the corresponding eigenstates (the 000a00 series) will play a very important role in this paper. Another set of Fermi resonance doublets concerning the 000a00 series is of the type $010a00/000(a+2)00$. Even though the energy difference of the corresponding harmonic eigenstates is about 90 cm^{-1}, the resonant character rapidly increases with a such that an assignement by means of harmonic quantum numbers for $a > 2$ is rather arbitrary for this pair. It should be added that the 000a00 overtones contain a considerable admixture of the HON local mode as almost all eigenfunctions do for *cis* HONO. To illustrate the statment that the energy optimal path corresponds to the 000a00 series we have depicted in Figure 2 this path in dashed line overlayed with the reduced density plots of the 010(a-2)00/000a00 pairs with a = 2, 3, 4, 5. A visual inspection of Figure 2 confirms that the most efficient isomerization pathway corresponds to the excitation of this series.

Similary to 000010/000100, the fundamentals refered to as N=O (010000) and HON (001000) fundamentals are both rather a mixture of both local modes. But in this case the effects due to resonances are much less pronounced and no inversion of ordering appears. Hence, the small c^2_{harm} value for 001000 result from another type of resonance:

probably a resonance of the type $abcdef/ab(c-1)de(f+2)$ whose pairs are likely to present resonant doublets. Indeed, the energy difference between the corresponding harmonic eigenstates is about 6 cm^{-1}.

The vibrationally averaged dipole moments are also given in Tables II, III and IV for the calculated vibrational states of the symmetry A'. The averaged value on the ground state of the dipole moment is of 0.5718 a.u and its angle with the a principal axis of the inertia tensor (making itself an calculated angle of 26.9° with the ON-axis) is of 73.2°. They are in reasonable agreement with the experimental values (0.5599 a.u. and 77.6° [61], respectively). The angles between the transition dipole moments and the a principal axis were calculated to be of 11.4°, 16.5°, 2.0°, 79.6° for the fundamental transitions: ν_k k←0 (k=5,4,2,1). They are in rather good agreement with those calculated in Ref. [62] (7.0°, 17.5°, 5.5°, 81.9°, respectively). They also confirm the findings of [63] that among the observed bands only the ν_1 transition is nearly of b principal axis type in cis-HONO. We predict that the (until now not observed) ν_3 band to be also nearly of b type with 70.7° (72 ° in Ref. [62]) between the transition dipole moment and the principal axis of the inertia tensor.

We have also calculated transition intensities in km/mol using the following formula [62, 64]:

$$S_{if} = 2.50643\,\nu_{if}\sum_\alpha \langle i|\mu_\alpha|f\rangle^2 \tag{14}$$

with $E_{if} = E_f - E_i$, $f > i$ and ν_i beeing the energy of the i'th eigenstate.

TABLE V AROUND HERE

The results for $i = 0$ are given in Table V. They are in good agreement with the only existing experimental value and in reasonable agreement with the previous theoretical predictions given in Table V. Inspection of the components of the transition moments from the ground state in Tab. II reveals that restricting the radiation on z direction favors excitation of 000a00 against other transitions. Since this choice of the laser parameters should favour the excitation of the middle-ON stretch it would make sense here to characterize 000100 as

the ON mode, as generally proposed in the literature.

Figure 3 depicts all transition moments between all levels for the z-component of μ (do not forget that we want to excite the middle-ON stretch to trigger the $cis \rightarrow trans$ isomerization and thus to use a laser pulse in the z direction: see section II B). Three sets of values can be distinguished. The first, the second and the third set include transitions between levels whose energy difference is around 600 cm^{-1}, 850 cm^{-1}, and 1630 cm^{-1}, respectively. They correspond to (a) $\langle abcdxf|\mu_z|abcd(x+1)f\rangle$, (b) $\langle abcxef|\mu_z|abc(x+1)ef\rangle$, and (c) $\langle axcdef|\mu_z|a(x+1)bcdef\rangle$-type transitions, respectively. Other excitation pathways are much less efficient for z polarised laser radiation. This suggests to use fixed laser frequencies of about 600 or about 850 cm^{-1} in order to excite roughly the (a) or the (b) series, respectively, by a (possibly successive) multiphoton process. Indeed, both series include comparably high transition moments. Very important for the efficiency of the isomerization which is the stake in this work, the (b) series has fortunatly the largest intensities compared to the other series. We have also plotted figures similar to Figure 3 but for the x or y components and noticed that the transitions of the series (b) are appreciably smaller for the x or y components (on the other hand the transitions of the series (a) increase) so that we are confident that a laser pulse parallel to the z^{BF} axis is optimal to excite the $Q^+_{ONO/ON}$ motion.

We have calculated the $trans$ eigenstates in A'-symmetry using the same procedure as for the cis eigenstates. The results are presented in Table VI, VII, VIII, IX and X. The

comparison with the previously calculated levels (ref. [21]) lead to the same conclusions as for the *cis* geometry. In particular, the N=O stretch fundamental 010000 is lowered by 8 cm^{-1} using the *improved* relaxation method and the unmodified PES. As for the *cis* geometry, the ON (000100) stretch and the ONO bend (000010) fundamentals can be described as a symmetric (000100) and antisymmetric (000010) superposition of local ON and ONO modes. However, in contrast to the *cis* HONO geometry, fermi-resonances are generally much less pronounced. Consequently, the square harmonic coefficients are larger than 0.5 at least for the fundamentals. In particular, the HON bend fundamental and overtones have no resonant character. They have a very local HON bend character.

We have also found a few delocalised pairs which correspond to *cis-trans* resonances, i.e. pairs levels close in energy with an unexpected strong delocalisation. The latter can only be explained by a resonance between the *cis* and *trans* eigenfunctions. To be more specific, *trans*-000312 (3883.4 cm^{-1})/*cis*-002200 (3880.2 cm^{-1} relative to the *trans* ground state) and *trans*-010004 (3681.9 cm^{-1})/ *cis*-000302(3675.0 cm^{-1} relative to the *trans* ground state) can be characterised by such *cis-trans* resonance pairs. In the isomerization, these pairs only play a minor role, since they can not be efficiently excited (they are combination bands). For the sake of completenes, transition energies and moments for the *trans* geometry are given in Table X. The transition intensities for the fundamentals are compared to the experimental values and to calculated values from other works. They are in reasonable agreement with both.

VI. EXCITATION AT 850 cm^{-1} LASER FREQUENCY

In section IIB, we have stated that we will start from the ground state of the *cis* geometry (since the *cis*→ *trans* isomerization is much faster than the opposite direction). Furthermore, we found that an efficient isomerization is expected when a wave packet motion is induced introducing a simultaneous increase of R_3 and $cos(\theta_2)$. This exactly corresponds to the excitation of the (b) series in Figure 3 using a laser frequency of about 850 cm^{-1}. Since the transition moments of the (b) series are highest for the z component of the dipole field, the optimal oriention of the laser is parallel to the z^{BF} axis (see Section V), i.e. parallel to the middle-ON bond. Consequently, we will use z-polarised laser fields with frequencies of about 850 cm^{-1}.

Ideally, the dynamics should proceed as follows: a periodic motion along the optimal $(R_3, \cos(\theta_2))$ path is induced by the laser field. Each time the meanvalues of the two coordinates R_3 and $\cos(\theta_2)$ reach their maximal values B_τ becomes minimal and pronounced irreversible isomerization takes place. This mechanism is extremely selective since the desired reaction is thought to be finished before the major part of the energy is redistributed. Interestingly enough, similar arguments can hold for the *trans* to *cis* isomerization (which is not investigated in detail in this paper since as shown in Ref. [22], the *trans* to *cis* is far less efficient). There is, however, a marked difference. Indeed, it is now the opposite direction, i.e. 'asymetric' $Q^-_{ONO/ON}$ direction, and hence the 0000a0 series, which induces the *trans* to *cis* isomerization. The decrease of B_τ in this second case, due to the $Q^-_{ONO/ON}$ motion, is less pronounced than for the the *cis* to *trans* isomerization (The definition of B_τ for the trans case differs from eq. (5) by setting $\tau = 180$). This disymmetry is very important for it will prevent the wavepacket from returning to the *cis* geometry and thus ensures a partial irreversibility of the *cis* to *trans* isomerization.

As aforementioned, we wish to induce quasiclassical motion of large amplitude in the $Q^+_{ONO/ON}$ direction, implying a large number of excited eigenstates of type (b) (cf. Figure 3), preferably 000a00 and 010(a-2)00. Of course, a compromise has to be found between a short time/high field strength and a long time/low field strength propagation. The first may indeed result in pronounced excitations of eigenstates different from the b-type. On the

other hand, with a low field strength, it can become very intricate to coherently populate even a sufficient number of the desired overtones, albeit more selective population is possible. When pulse widths of individual transitions (which are directly linked to the field strength) become smaller than the level spacings between the eigenstates, the absorbtion becomes very sensitive to the choosen frequency. It may then happen, that a proper frequency for a desired multiphoton excitation cannot be found at all. A systematic study of this problem for multiphoton mechanisms using model systems is presented in [65]. In our case, we found that the values 0.0035 a.u. for the field strength and 500 fs for the irradiation time are sufficiently good candidates for exciting HONO, although these values could be, of course, further optimised (see below). The final total energy was about 1.05 eV.

FIGURE 4 AROUND HERE

FIGURE 5 AROUND HERE

In Figure 4, the squared overlapps between the wavepacket after excitation by the previously defined laser field ($E_0 = 0.0035$ a.u., $\omega = 850$ cm^{-1}, and $t_p = 500$ fs) and all converged eigenfunctions up to around 4000 cm^{-1} are depicted. The Fourier transform of the autocorrelation function (up to 5000 cm^{-1}) is also displayed on the same figure. A series of groups of levels with about 850 cm^{-1} energy difference between each group crops up. The main contributions in each group correspond to the following eigenstates: (0: 000000), (I: 000100/...), (II: 000200/010000/..), (III: 000300/010100/001002/..), (IV: 000400/010200/001120/000024 ...), (V: 000500/010300/011020/000124/...) at about 850, 1685, 3290, and 4065 cm^{-1}, respectively. The last two group most likely contain also 000600/010400 and 000700 as main contributions, but it was impossible to converge the corresponding eigenfunctions. Figure 4 explicitely demonstrates that the external field leads to a very different excitation from the one of Ref. [22] obtained by an artificial excitation of the ON stretch: compare Figure 2 (b) in Ref. [22] with Figure 4. This justifies the importance of adding a laser pulse in the dynamics in order to be closer to experimental conditions. Moreover, Figure 5 shows that this process is a *successive or stepwise* multi photon one. We have noticed that the excitation process is relatively robust against variation of the excitation energy. In the range of 830-870 cm^{-1} for the excitation frequency, we have obtained roughly the same resulting spectrum and absorbed energy

(see also the discussion with the chirped laser below with frequencies ranging from 889 to 850 cm^{-1}). This is most likely due to the pulse width beeing larger than the level spacing within each group at the chosen field strength, or, in other words, due to the relatively large density of states in each group of levels.

FIGURE 6 AROUND HERE

In Figure 6, the evolution of the scaled meanvalues of the internal coordinates and P_{trans} is shown during the 500 fs radiation. As expected, $< R_3 >$ and $< cos(\theta_2) >$ oscillate in phase. Their meanvalues take the extremal values of 3.0 bohr and -0.25, corresponding roughly to a mean torsional barrier B_τ of about 1900 cm^{-1} (the values at the equilibrium geometry are 2.6 3.0 bohr and -0.39). The sudden changes of P_{trans} are clearly correlated to the oscillations of R_3 and $cos(\theta_2)$ as long as the wave packet remains fairly localised.

FIGURE 7 AROUND HERE

Figure 7 summarizes the whole process: we have plotted a two-dimensional section of the potential hypersurface of HONO including the two minima and the saddle point. The abscissa correponds to τ and the ordinate to R_3. The lowest contour line corresponds to 0.017 eV and the highest one to 2. eV. Depicted are also snapshots of the evolution of reduced dimensionality probability densities of HONO between 290 and 400 fs after excitation start. Figure 7 shows that the wave packet performs a localized motion in the initial phase of the excitation with the laser pulse (t = 290 and 305 fs): excitation along the z axis leads to regular oscillations along the optimal direction. The averaged value of R_3 is smaller than the value at the equilibrium geometry for 290 fs and larger for 305 fs. When the averaged value of R_3 becomes larger the wave packet starts to delocalize in the τ direction towards the *trans* geometry (t = 315 fs). This is perfectly coherent with the discussion in Section II B, since t = 315 fs corresponds to a low value of B_τ. The absorbed energy is thus sufficient to allow for a motion of the wave packet over the inversion barrier (t = 325 and 350 fs). After 350 fs, the system has absorbed a larger amount of energy and the population in the *trans* is larger (t = 370 and 400 fs). The part of the wave packet in the *trans* potential well is spread out and several maxima of probability appear.

21

Figure 8 around here

Figure 9 around here

Furthermore, Figure 8 which provides the evolution of the expectation values of the coordinates ON and ONO after the irradiation suggests that this induced process continues (albeit less pronounced) also during the IVR, i.e. when the laser field is off after 500 fs. Note that the "in phase" motion of the HON bend is due to the nature of the 000a00 overtones (see above the analysis of the spectrum). Let us now turn to a detailed description of the dynamics over the first 2500 fs and in terms of the energies of the harmonic modes which are depicted in Figure 9. The calculation of these energies was performed as in Ref. [31], i.e. after having defined curvilinear normal modes (see section V in the present work and section C.2 in Ref. [31]). At 2500 fs around 35 % of the energy was deposited in the $Q^+_{ONO/ON}$ harmonic mode, 20 % in the torsional mode. On the other hand, at 2500 fs, we find around 20 % of the energy in the N=O stretch, 15 % in the HON bend, and 10 % in the $Q^-_{ONO/ON}$ mode. We can thus say that about 55 % of the energy is utilized for the isomerization. The above proposed mechanism can therefore be considered as rather selective. Finally, it is important to notice that a quasiperiodic energy flow between the $Q^+_{ONO/ON}$ and the N=O harmonic modes is observed revealing a resonance between these two modes. This is consistent with the analysis of the eigenstates (see section V) where a Fermi resonance of the type $010a00/000(a+2)00$ was described. Unfortunately for the purpose of our work, it is impossible to induce a regular motion in $Q^+_{ONO/ON}$ direction without exciting the N=O stretch and the HON bend at the same time. Consequently, the strong mode coupling in HONO prevents a highly selective process. While periodic excitation of N=O stretch only delays the isomerization, the energy deposited in the HON bend is almost completely lost for the isomerization. If we now compare with the artificial excitation of the local ON mode in Ref. [22], we see that the latter was more selective excluding almost all the modes from excitations except ON and ONO. On the other hand, the local ON mode in Ref. [22] consists of a mixture of 000a00 and 0000a0 eigenfunctions which is less effective for isomerization than the 000a00 series alone obtained by the excitation by the laser field in this work. This explains roughly the similar isomerization rates for both processes. Let us return to Figure 9 : about 900 cm^{-1} of energy is transfered into the torsional mode during the whole process. This is not surprising since the spectrum up to 4000 cm^{-1}

(Figure 4) shows excited groups which contain combination bands of the ON, ONO and the torsional modes. In the higher energy part of the spectrum one can also expect such combination bands to be excited. The highest excited eigenstates have a stronger tendancy to delocalize into the *trans* well. Within the dynamic picture this transfer can be mainly understood considering the potential couplings $Q^+_{ONO/ON}$-torsion (see Section II B). Note that the energy transfer into the torsional coordinate here is somewhat higher (> 800 cm^{-1}) compared with our previous work [22] during the corresponding propagation after an artificial excitation of the ON stretch.

In order to check the robustness of the described mechanism against variations of the frequency we have used a laser pulse chirped from the harmonic ν_5 frequency 889 cm^{-1} to the anharmonic one at 850 cm^{-1}. We found that an field strength of 0.003 a.u. was sufficient to excite the molecule to 1.02 eV of total energy in the chirped case. Except that the chirped pulse is a little bit more efficient, we have noticed that the same mechanism was induced to the system resulting in about $P_{trans} = 13$ % isomerization after 2 ps. As aforementioned, this confirms that the excitation process is relavively robust against variations of the excitation energy.

Furthermore, we excited the molecule to higher total energies using higher laser intensities, but the same time duration of the laser pulse and a fixed frequency of 850 cm^{-1}. In order to compare both the rapidity of the isomerization and final isomerization yield for all the processes we have fitted the survival propabilities $1 - P_{trans}(t)$ to the expression :

$$1 - P_{trans}(t) = exp(-kt)P^F_{trans} + (1 - P^F_{trans}), \quad t > 500 fs \qquad (15)$$

where the rate constant k and final trans probability $P_{trans}(t \rightarrow \infty) = P^F_{trans}$ were optimized. The root mean square error of the fit shows that this expression provides a reasonable description of P_{trans}. Hereby, we have not used points of $P_{trans}(t)$ for $t < 500$ fs, since during the excitation $P_{trans}(t)$ is not expected to follow our model function. (Note that the model function is fixed at 1 for $t = 0$ anyway). The results in Table XI give a fair idea about the trends for higher total energies. The final *trans* probability P^F_{trans} roughly linearly increases with increasing absorbed energy within the considered energy range. The reaction time propational to $1/k$ also decreases roughly linearly with increasing total energy.

23

To give an estimate of the expected final trans-probability for an experiment with free orientation, we have also propagated for other orientations than z. We found no isomerisation for x and y polarisations for 0.0035 a.u. field strengh. Orientation of 45 deg. between the x and y axis yields about the half of the final P_trans of the z polarised case. Thus, asuming isotropic orientation during the laser irradiation one can roughly estimate that only one third of the calculated P_trans will be observed.

VII. CONCLUSIONS

We have investigated the $cis \rightarrow trans$ insomerization in HONO with an external time-dependent field using a realistic PES and a realistic dipole moment function. A full quantum mechanical approach was adopted. The main results are summarized as follows:

- (i) we have determined an efficient *selective* IVR-pathway leading to the $cis \rightarrow trans$ isomerization. This path corresponds to a simultaneous increase of the (middle) ON stretch and of the ONO bending.

- (ii) we have calculated a realistic six-dimensional dipole moment surface and calculated all the vibrational eigenstates up to 4000 cm^{-1} using our previously developped PES and the improved relaxation method of MCTDH. We have observed that the selective IVR-pathway corresponds to an excitation of the 010a00/000(a+2)00 series of eigenstates (see table I and section V for the definition of the normal and local modes).

- (iii) we have simulated the dynamics with MCTDH and in presence of laser pulse with a carrier frequency of 850 cm^{-1}, an intensity of 0.0035 a.u., and an irradiation duration of 500 fs. We have observed the isomerization process and the fact that the process is relatively robust against variation of the excitation frequency.

- (iv) in section II, we have detailed the model which constitutes the framework of this work indicating all our approximations. We predict that HONO isomerizes in gas phase with a yield of about 10 percent when the suggested parameters for the pulse are used. Higher yields are likely if higher intensities or longer irradiation times are used.

Acknowledgements

[1] P. A. McDonald and J. S. Shirk. The infrared laser photoisomerization of HONO in solid N_2 and Ar. *J. Chem. Phys.* **77** (1982), 2355.

[2] A. E. Shirk and J. S. Shirk. Isomerization of HONO in solid nitrogen by selective vibrational excitation. *Chem. Phys. Lett.* **97** (1983), 549–552.

[3] L. Khriatchev, J. Lundell, E. Isoniemi, and M. Räsänen. HONO in solid Kr: Site-selective transcis isomerization with narrow-band infrared radiation. *J. Chem. Phys.* **113** (2000), 4265–4273.

[4] J. M. Guilmot, M. Carleer, M. Godefroid, and M. Herman. *J. Mol. Spec.* **143** (1990), 81.

[5] J. M. Guilmot, M. Godefroid, and M. Herman. The rovibrational spectrum of trans-HNO_2. *J. Mol. Spec.* **160** (1993), 387–400.

[6] J. M. Guilmot, F. Mélen, and M. Herman. The rovibrational spectrum of cis-HNO_2. *J. Mol. Spec.* **160** (1993), 401–410.

[7] R. Schanz, V. Botan, and P. Hamm. A femtosecond study of the infrared-driven cis-trans isomerization of nitrous acid (hono). *J. Chem. Phys.* **122** (2005), 044509.

[8] V. Botan, R. Schanz, and P. Hamm. The infrared-driven cis-trans isomerization of hono. ii: Vibrational relaxation and slow isomerization channel. *J. Chem. Phys.* **124** (2006), 234511.

[9] K. K. Lehman, G. Scoles, and B. H. Pate. *Ann. Rev. Phys. Chem.* **45** (1994), 241.

[10] T. Uzer. *pr* **73** (1991), 73.

[11] M. Quack. *Ann. Rev. Phys. Chem.* **41** (1990), 839.

[12] R. E. Wyatt, C. Iung, and C. Leforestier. Quantum dynamics of overtone relaxation in benzene. I. 5 and 9 modes models for relaxation from CH($\nu = 3$). *J. Chem. Phys.* **97** (1992), 3458.

[13] R. E. Wyatt, C. Iung, and C. Leforestier. Quantum dynamics of overtone relaxation in benzene. II. 16 mode models for relaxation from CH($\nu = 3$). *J. Chem. Phys.* **97** (1992), 3477.

[14] C. Iung, C. Leforestier, and R. E. Wyatt. *J. Chem. Phys.* **98** (1993), 6722.

[15] R. E. Wyatt and C. Iung. Quantum dynamics of overtone relaxation in benzene. V. CH($\nu = 3$) dynamics computed with a new ab initio force field. *J. Chem. Phys.* **98** (1993), 6758.

[16] R. E. Wyatt and C. Iung. *J. Chem. Phys.* **101** (1994), 3671.

[17] C. Iung and R. E. Wyatt. Time-dependent quantum mechanical studyy of intramolecular

vibrational energy redistribution in benzene. *J. Chem. Phys.* **99** (1993), 2261–2264.

[18] R. E. Wyatt, C. Iung, and C. Leforestier. *Acc. Chem. Res.* **28** (1995), 423.

[19] A. Maynard, R. E. Wyatt, and C. Iung. A quantum dynamical study of CH overtones in fluoroform. II. Eigenstate analysis of the $v(\text{CH}) = 1$ and $v(\text{CH}) = 2$ regions. *J. Chem. Phys.* **106** (1997), 9483.

[20] T. J. Minehardt and R. E. Wyatt. Quasiclassical dynamics of benzene overtone relaxation on an ab initio force field. I. Energy flow and survival probabilities in planar benzene for CH(v = 2,3). *J. Chem. Phys.* **109** (1998), 8330.

[21] F. Richter, M. Hochlaf, P. Rosmus, F. Gatti, and H.-D. Meyer. A study of mode–selective trans–cis isomerisation in HONO using ab initio methodology. *J. Chem. Phys.* **120** (2004), 1306–1317.

[22] F. Richter, P. Rosmus, F. Gatti, and H.-D. Meyer. Time–dependent wavepacket study on trans–cis isomerisation of HONO. *J. Chem. Phys.* **120** (2004), 6072–6084.

[23] Y. Guan, G. C. Lynch, and D. L. Thompson. Intramolecular energy transfer and cistrans isomerization in HONO. *J. Chem. Phys.* **87** (1987), 6957–6966.

[24] Y. Guan and D. L. Thompson. Mode specificity and the influence of rotation in cis-trans isomerization and dissociation in HONO. *Chem. Phys.* **139** (1989), 147–161.

[25] Y. Qin and D. L. Thompson. Classical dynamics study of HONO using constrained trajectories. *J. Chem. Phys.* **96** (1992), 1992–1999.

[26] Y. Qin and D. L. Thompson. Semiclassical treatment of tunneling effects in HONO cistrans isomerization. *J. Chem. Phys.* **100** (1994), 6445–6457.

[27] P. M. Agrawal, D. L. Thompson, and L. M. Raff. Theoretical studies of the effects of matrix composition, lattice temperature, and isotopic substitution on isomerization reactions of matrix-isolated HONO/Ar. *J. Chem. Phys.* **102** (1995), 7000–7005.

[28] Y. Guo and D. L. Thompson. A theoretical study of cistrans isomerization in hono using an empirical valence bond potential. *J. Chem. Phys.* **118** (2003), 1673–1678.

[29] F. Gatti and H.-D. Meyer. Intramolecular vibrational energy redistribution in Toluene: A nine dimensional quantum mechanical study using the MCTDH algorithm. *Chem. Phys.* **304** (2004), 3–15.

[30] C. Iung, F. Gatti, and H.-D. Meyer. Intramolecular vibrational energy redistribution in the highly excited Fluoroform molecule: A quantum mechanical study using the MCTDH

algorithm. *J. Chem. Phys.* **120** (2004), 6992–6998.

[31] G. Pasin, F. Gatti, C. Iung, and H.-D. Meyer. Theoretical investigation of Intramolecular Vibrational Energy Redistribution in highly excited HFCO. *J. Chem. Phys.* **124** (2006), 194304.

[32] G. Pasin, F. Gatti, C. Iung, and H.-D. Meyer. *J. Chem. Phys.* **126** (2007), 024302.

[33] H.-D. Meyer, F. Le Quéré, C. Léonard, and F. Gatti. Calculation and selective population of vibrational levels with the Multiconfiguration Time-Dependent Hartree (MCTDH) algorithm. *Chem. Phys.* **329** (2006), 179–192.

[34] H.-D. Meyer, U. Manthe, and L. S. Cederbaum. The multi-configurational time-dependent Hartree approach. *Chem. Phys. Lett.* **165** (1990), 73–78.

[35] U. Manthe, H.-D. Meyer, and L. S. Cederbaum. Wave-packet dynamics within the multiconfiguration Hartree framework: General aspects and application to NOCl. *J. Chem. Phys.* **97** (1992), 3199–3213.

[36] M. H. Beck, A. Jäckle, G. A. Worth, and H.-D. Meyer. The multiconfiguration time-dependent Hartree method: A highly efficient algorithm for propagating wavepackets. *Phys. Rep.* **324** (2000), 1–105.

[37] H.-D. Meyer and G. A. Worth. Quantum molecular dynamics: Propagating wavepackets and density operators using the multiconfiguration time-dependent Hartree (MCTDH) method. *Theor. Chem. Acc.* **109** (2003), 251–267.

[38] R. Loudon. *The Quantum Theory of Light.* Oxford University Press, Oxford, 1983.

[39] S. Hervé, F. Le Quéré, and R. Marquardt. Effect of rotations on the generation of coherent internal molecular motion. *Int. J. Quant. Chem.* **99** (2004), 439.

[40] H. J. Loesch and A. Reimscheid. *J. Chem. Phys.* **93** (1990), 4779.

[41] A. Slenszka, B. Friedrich, and D. Herschbach. *Phys. Rev. Lett.* **72** (1994), 1806.

[42] W. KIm and P. M. Felker. *J. Chem. Phys.* **104** (1996), 1147.

[43] L. Cai, J. Marango, and B. Friedrich. *Phys. Rev. Lett.* **86** (2001), 775.

[44] T. Seideman. *J. Chem. Phys.* **115** (2001), 5965.

[45] R. Marquardt, M. Quack, I. Thanopoulos, and D. Luckhaus. Tunneling dynamics of the nh chromophore in nhd$_2$ during and after coherent infrared excitation. *J. Chem. Phys.* **118** (2003), 643–658.

[46] H. L. Bethlem, G. Berden, F. M. Crompvoets, R. T. Jongma, A. J. A. van Roij, and G. Meijer.

29

Nature **406** (2000), 491.

[47] F. Gatti. Flexible monomer formulation for non-rigid systems. *Chem. Phys. Lett.* **373** (2003), 146–152.

[48] A. Nauts and X. Chapuisat. *Chem. Phys. Lett.* **136** (1987), 164.

[49] F. Gatti, Y. Justum, M. Menou, A. Nauts, and X. Chapuisat. Quantum-mechanical description of rigidly or adiabatically constrained molecular systems. *J. Mol. Spec.* **373** (1997), 403.

[50] D. Lauvergnat and A. Nauts. *J. Chem. Phys.* **116** (2002), 8560.

[51] C. Leforestier, F. Gatti, R. S. Fellers, and R. J. Saykally. Determination of a flexible (12D) water dimer potential via direct inversion of spectroscopic data. *J. Chem. Phys.* **117** (2002), 8710.

[52] C. Eckart. *Phys. Rep.* **47** (1935), 552.

[53] S. Hervé, F. Le Quéré, and R. Marquardt. *J. Chem. Phys.* **114** (2001), 826.

[54] S. Hervé, F. Le Quéré, and R. Marquardt. *J. Chem. Phys.* **116** (2002), 3300.

[55] F. A. Hamprecht, A. J. Cohen, D. J. Tozer, and N. C. Handy. *J. Chem. Phys.* **109** (1998), 6264.

[56] R. D. Amos, I. L. Alberts, J. S. Andrews, S. M. Colwell, N. C. Handy, D. Jayatilaka, P. J. Knowles, R. Kobayashi, K. E. Laidig, G. Laming, A. M. Lee, P. E. Maslen, C. W. Murray, J. E. Rice, E. D. Simandiras, A. J. Stone, M.-D. Su, and D. J. Tozer. The Cambridge Analytic Derivatives Package, Issue 6.5, (2001). See http://www-theor.ch.cam.ac.uk/software/cadpac.html.

[57] T. H. Dunning. *J. Chem. Phys.* **55** (1971), 716.

[58] G. A. Worth, M. H. Beck, A. Jäckle, and H.-D. Meyer. The MCTDH Package, Version 8.2, (2000). H.-D. Meyer, Version 8.3 (2002). See http://www.pci.uni-heidelberg.de/tc/usr/mctdh/.

[59] S. Carter and N. C. Handy. *Mol. Phys.* **1673** (2002), 681.

[60] D. Luckhaus. The vibrational spectrum of HONO: Fully coupled 6D direct dynamics. *J. Chem. Phys.* **118** (2003), 8797–8806.

[61] A. P. Cox, A. H. Brittain, and D. J. Finningan. *Trans. Faraday Soc.* **67** (1971), 2179.

[62] V. P. Bulychev and K. G. Tokhadze. Multidimensional anharmonic calculation of the vibrational frequencies and intensities for the *trans* and *cis* isomers of hono with the use of normal

coordinates. *J. Mol. Struct. (Theochem)* **708** (2004), 47.

[63] C. M. Deely and I. M. Mills. The infrared vibration-rotation spectrum of *trans* and *cis* nitrous acid. *J. Mol. Struct. (Theochem)* **100** (1983), 199.

[64] A. Willets, N. C. Handy, W. H. Green, , and D. Jayatilaka. *J. Phys. Chem.* **94** (1990), 5604.

[65] E. A. Donley, R. Marquardt, M. Quack, J. Stohner, I. Thanopulos, and E.-U. Wallenborn. Some simple mechanisms of multiphoton excitation in many-level systems. *Mol. Phys.* **99** (2001), 1275–1287.

[66] T. J. Lee and A. P. Rendell. *J. Chem. Phys.* **94** (1991), 6229.

TABLE I: Calculated harmonic frequencies of the different vibrational modes and comparison of calculated and experimental transition energies in cm^{-1} for the *cis* geometry.

Frequencies	harmonic [a]	Mode	obs.[b]	MCTDH [c]
ω_1 (OH)	3652.6	ν_1	3426	3438.5
ω_2 (N=O)	1679.6	ν_2	1641	1632.0
ω_3 (HON)	1356.7	ν_3		1311.6
ω_4 (ON)	889.8	ν_4	852	850.1
ω_5 (ONO)	651.6	ν_5	609	616.7
ω_6 (out-of-plane)	675.5	ν_6		
		$2\nu_6$		1212.7

[a]Harmonic frequencies from Ref. [21].
[b]Experimental values taken from Ref. [6].
[c]This work with the *improved relaxation* method.

TABLE II: Vibrational levels (A') 'rlx' obtained with the *improved relaxation* method and cis-probabilities (P_{cis}) of *cis*-HONO. Energies are relative to the ground-state of the *trans*-HONO. c^2_{harm} is the square of the overlap between the eigenstate and the nearest harmonic eigenstate. Δvar. is the difference E_{rlx}-E_{var}, E_{var} beeing the results of Ref. [21] obtained by the variational method (see text). Given are the averaged values $\mu_x^{ii} =< i|\mu_x|i >$, $\mu_z^{ii} =< i|\mu_z|i >$, $\mu_x^{0i} =<GS|\mu_x|i >$ and $\mu_z^{0i} =<GS|\mu_z|i >$ of the x and z components of the dipole moment vector. S is the transition intensity from the ground state to the corresponding excited state. S_z is its z component only.

| rlx | Δvar. | P_{cis} | c^2_{harm} | μ_x^{ii} | μ_z^{ii} | μ_x^{0i} | μ_z^{0i} | S | S_z |
[cm^{-1}]	[cm^{-1}]			[a.u.]	[a.u.]	[a.u.]	[a.u.]	[$\frac{km}{mol}$]	[$\frac{km}{mol}$]
000000 94.0	-3.11	1.0000	0.830	0.413	-0.395	0.4132	-0.3952	-	-
000010 616.7	0.36	1.0000	0.519	0.424	-0.368	-0.0361	-0.0456	33.8	41.5
000100 850.1	0.44	1.0000	0.487	0.421	-0.358	-0.0260	-0.1404	280.8	543.0
000002 1212.7	0.75	1.0000	0.599	0.408	-0.354	-0.0012	-0.0026	0.2	0.3
000020 1218.8	0.57	1.0000	0.253	0.434	-0.336	0.0050	0.0070	1.5	2.0
001000 1311.6	-1.05	1.0000	0.472	0.412	-0.381	0.0186	-0.0025	7.5	0.3
000110 1453.5	0.66	1.0000	0.267	0.432	-0.329	-0.0020	-0.0106	2.7	5.2
010000 1632.0	-7.46	1.0000	0.557	0.402	-0.411	-0.0396	-0.0717	177.4	271.8
000200 1685.4	0.21	1.0000	0.216	0.427	-0.326	-0.0134	-0.0205	16.4	22.9
000030 1803.6	0.71	1.0000	0.126	0.446	-0.302	0.0008	0.0022	0.2	0.3
000012 1808.9	0.63	1.0000	0.307	0.421	-0.313	0.0014	0.0046	0.7	1.2
001010 1908.4	0.84	1.0000	0.186	0.424	-0.349	0.0003	0.0092	2.6	5.2
000102 2026.0	0.96	1.0000	0.326	0.412	-0.311	-0.0013	-0.0001	0.1	0.0
000120 2042.3	0.53	1.0000	0.101	0.443	-0.296	0.0014	0.0029	0.3	0.6
001100 2146.9	-1.02	1.0000	0.170	0.420	-0.347	-0.0026	0.0008	0.3	0.1
010010 2245.3	-6.85	1.0000	0.232	0.413	-0.381	-0.0033	-0.0042	1.1	1.3
000210 2276.5	0.44	1.0000	0.083	0.437	-0.299	0.0009	0.0001	0.0	0.0
000004 2282.5	-1.95	1.0000	0.511	0.392	-0.293	0.0001	0.0007	0.0	0.0
000040 2372.6	0.30	1.0000	0.038	0.463	-0.260	0.0001	0.0002	0.0	0.0
000022 2384.6	-1.02	1.0000	0.138	0.430	-0.269	-0.0001	-0.0004	0.0	0.0
010100 2471.5	-5.16	1.0000	0.134	0.416	-0.353	0.0009	0.0030	0.4	0.7
001020 2488.2	-1.12	1.0000	0.049	0.437	-0.312	-0.0002	0.0003	0.0	0.0
001002 2499.1	-2.73	1.0000	0.275	0.407	-0.343	-0.0018	0.0038	0.7	1.2
000300 2511.0	-2.70	1.0000	0.055	0.427	-0.314	0.0000	0.0010	0.0	0.1

TABLE III: Continuation of Table II.

	rlx	Δvar.	P_{cis}	c^2_{harm}	μ_x^{ii}	μ_z^{ii}	μ_x^{0i}	μ_z^{0i}	S	S_z
	[cm^{-1}]	[cm^{-1}]			[a.u.]	[a.u.]	[a.u.]	[a.u.]	[$\frac{km}{mol}$]	[$\frac{km}{mol}$]
000112	2600.3	-3.01	1.0000	0.058	0.418	-0.303	0.0015	-0.0035	0.6	1.0
002000	2608.3	-2.41	1.0000	0.117	0.417	-0.322	-0.0017	0.0036	0.7	1.1
000130	2615.6	-1.00	1.0000	0.014	0.454	-0.261	-0.0002	-0.0009	0.0	0.1
001110	2728.7	-2.12	1.0000	0.049	0.432	-0.313	0.0004	-0.0006	0.0	0.0
000202	2812.8	-5.50	0.9892	0.087	0.404	-0.270	-0.0003	-0.0001	0.0	0.0
000014	2835.6	-5.24	0.9952	0.059	0.393	-0.302	-0.0014	-0.0008	0.1	0.1
000220	2841.6	-5.50	1.0000	0.012	0.441	-0.290	-0.0003	0.0000	0.0	0.0
010002	2845.2	-6.81	0.9981	0.212	0.403	-0.306	-0.0010	-0.0006	0.1	0.0
010020	2854.8	-4.70	0.9998	0.053	0.425	-0.325	0.0010	0.0006	0.1	0.0
000050	2922.8	-1.80	1.0000	0.004	0.478	-0.216	0.0001	-0.0002	0.0	0.0
011000	2930.1	-9.40	1.0000	0.301	0.401	-0.393	-0.0039	-0.0036	1.4	1.3
000032	2939.8	-2.90	0.9999	0.032	0.443	-0.218	0.0002	0.0001	0.0	0.0
001200	2969.5	-3.49	1.0000	0.028	0.425	-0.318	0.0010	0.0013	0.1	0.2
000104	3034.7	-9.92	0.8393	0.074	0.265	-0.285	-0.0001	-0.0001	0.0	0.0
001030	3048.9	-3.53	1.0000	0.006	0.450	-0.270	0.0000	0.0002	0.0	0.0
000310	3067.8	-4.50	1.0000	0.007	0.430	-0.308	0.0004	0.0004	0.0	0.0
001012	3073.2	-5.40	0.9999	0.092	0.416	-0.285	-0.0003	-0.0001	0.0	0.0
010110	3095.0	-5.70	1.0000	0.017	0.433	-0.297	-0.0001	-0.0003	0.0	0.0
000122	3158.0	-9.10	0.9197	0.009	0.358	-0.251	-0.0004	-0.0000	0.0	0.0
000006	3166.4	-6.59	0.8545	0.153	0.273	-0.227	-0.0022	0.0019	0.4	0.4
000140	3172.0	-5.90	0.9920	0.000	0.460	-0.225	-0.0001	-0.0000	0.0	0.0
002010	3180.6	-5.70	0.9773	0.044	0.403	-0.309	-0.0008	0.0000	0.0	0.0
020000	3237.8	-15.40	1.0000	0.349	0.391	-0.427	-0.0027	-0.0083	4.0	7.2
001120	3284.5	-6.50	0.9882	0.001	0.424	-0.272	-0.0001	-0.0004	0.0	0.0
000400	3292.0	-9.50	0.9993	0.003	0.422	-0.307	0.0010	0.0005	0.1	0.0
001102	3298.5	-12.30	0.9918	0.042	0.414	-0.285	0.0004	-0.0002	0.0	0.0
010200	3332.4	-7.06	0.9704	0.000	0.404	-0.294	-0.0011	-0.0011	0.1	0.1
000024	3357.3	-13.30	0.8396	0.001	0.287	-0.226	0.0001	-0.0000	0.0	0.0
000212	3382.5	-12.32	0.9593	0.007	0.385	-0.224	-0.0002	0.0001	0.0	0.0
000230	3413.0	-8.00	0.9995	0.000	0.461	-0.225	0.0001	0.0001	0.0	0.0
002100	3421.6	-8.70	0.9994	0.030	0.418	-0.331	-0.0029	0.0021	0.7	0.5

TABLE IV: Continuation of Tables II and III.

	rlx	Δvar.	P$_{cis}$	c$^2_{harm}$	μ$_x^{ii}$	μ$_z^{ii}$	μ$_x^{0i}$	μ$_z^{0i}$	S	S$_z$
	[cm^{-1}]	[cm^{-1}]			[a.u.]	[a.u.]	[a.u.]	[a.u.]	[$\frac{km}{mol}$]	[$\frac{km}{mol}$]
010030	3426.5	-9.10	0.9984	0.020	0.437	-0.305	0.0005	0.0003	0.0	0.0
100000	3438.1	0.40	1.0000	0.677	0.415	-0.402	-0.0143	0.0109	18.0	13.2
010012	3432.3	-9.95	0.9878	0.167	0.400	-0.328	0.0012	-0.0014	0.2	0.2
000060	3455.1	-6.73	1.0000	0.001	0.446	-0.180	0.0002	-0.0002	0.0	0.0
000042	3473.8	-7.99	0.9974	0.001	0.455	-0.167	0.0002	-0.0003	0.0	0.0
000114	3507.7	-23.24	0.8183	0.000	0.253	-0.241	-0.0000	0.0001	0.0	0.0
011010	3521.7	-11.69	0.9994	0.059	0.417	-0.339	0.0003	0.0008	0.1	0.1
001210	3535.7	-	0.9942	0.000	0.416	-0.293	0.0004	0.0002	0.0	0.0
001004	3554.6	-	0.8376	0.110	0.279	-0.273	0.0001	0.0001	0.0	0.0
000302	3581.0	-	0.5070	0.007	-0.057	-0.405	-0.0000	0.0000	0.0	0.0
001040	3591.0	-	0.8830	0.000	0.342	-0.261	0.0001	-0.0002	0.0	0.0
001022	3619.0	-	0.6578	0.011	0.135	-0.312	-0.0001	0.0000	0.0	0.0
000320	3640.0	-	0.9957	0.000	0.429	-0.294	0.0000	-0.0000	0.0	0.0
010102	3646.8	-	0.9491	0.163	0.363	-0.327	-0.0002	0.0003	0.0	0.0
010120	3670.4	-	0.8279	0.000	0.273	-0.300	0.0002	-0.0001	0.0	0.0
000132	3690.6	-	0.8668	0.001	0.330	-0.198	0.0000	-0.0000	0.0	0.0
000150	3712.1	-	1.0000	0.004	0.483	-0.182	0.0001	0.0000	0.0	0.0
002020	3731.5	-	0.9983	0.002	0.437	-0.272	-0.0000	-0.0000	0.0	0.0
001300	3750.2	-	0.9694	0.000	0.379	-0.238	-0.0001	0.0001	0.0	0.0
011100	3752.0	-	0.9893	0.040	0.396	-0.305	-0.0001	0.0002	0.0	0.0
002002	3760.5	-	0.9677	0.060	0.384	-0.298	0.0000	0.0000	0.0	0.0
002200	3786.2	-	0.7597	0.020	0.223	-0.351	-0.0000	0.0001	0.0	0.0
001130	3836.8	-	0.8114	0.003	0.173	-0.222	-0.0000	0.0000	0.0	0.0
020010	3846.8	-	0.9834	0.063	0.300	-0.249	0.0000	-0.0001	0.0	0.0
010210	3847.3	-	0.9467	0.007	0.395	-0.368	0.0003	0.0008	0.0	0.1
000410	3862.0	-	0.9483	0.000	0.385	-0.248	0.0000	-0.0001	0.0	0.0
003000	3879.5	-	0.8909	0.079	0.392	-0.261	-0.0000	0.0003	0.0	0.0
010004	3897.0	-	0.9796	0.283	0.147	-0.288	-0.0000	-0.0001	0.0	0.0
001112	3903.5	-	0.9468	0.000	0.322	-0.343	0.0000	0.0002	0.0	0.0
002110	3981.1	-	0.7027	0.001	0.367	-0.294	-0.0001	-0.0000	0.0	0.0
010040	4001.3	-	0.9434	0.002	0.392	-0.275	0.0002	0.0003	0.0	0.0

TABLE V: Comparison of calculated and experimental transition energies in cm^{-1} at the *cis* geometry. Given in parentheses are the transition moments in km/mol.

	ν_{exp} [a]	Calc.[b]	Calc.[c]	Calc. [d]	Calc. [e]	var. [f]	CCSD(T)/DFT [g]
000010	609	606(42)	592(37)	584(40)	620(46)	616.3	616.7(33.7)
000100	852(291)	854(296)	830(346)	841(214)	862(353)	849.7	850.1(281)
001000	-	1336(9)	1269(15)	1308(88)	1340(8)	1312.6	1311.6(7.5)
010000	1641	1641 (157)	1576(195)	1694(77)	1595 (136)	1639.5	1632.0(177)
100000	3426	3653(38)	3404(69)	3405(6)	3413(30)	3438.5	3438.1(18.0)
000002	-	-	1130(9)	1219(18)	1259(1)	1213.4	1212.7 (0.2)

[a]From Ref. [6]
[b]CCSD(T) calculations from Ref. [66].
[c](MP2/CC-VSCF)/HF 2D-anharmonic calculations from Ref. [3].
[d]DFT, 6D-anharmonic calculations from [60].
[e]MP2/3D-anharmonic from [62].
[f]From [21].
[g]This work.

TABLE VI: Vibrational levels (A') 'rlx' obtained with the *improved relaxation* method and trans-probabilities (P_{trans}) of *trans*-HONO. Energies are relative to the ground-state of *trans*-HONO. c_{harm}^2 is the square of the overlap between the eigenstate and the according harmonic eigenstate. Δvar. is the difference E_{rlx}-E_{var}, E_{var} beeing the results of Ref. [21] obtained by the variational method (see text). Given are the averaged values $\mu_x^{ii} = <i|\mu_x|i>$, $\mu_z^{ii} = <i|\mu_z|i>$, $\mu_x^{0i} = <GS|\mu_x|i>$ and $\mu_z^{0i} = <GS|\mu_z|i>$ of the x and z components of the dipole moment vector. S is the transition intensity from the ground state to the corresponding excited state. S_z is the transition intensity for a z-polarised laser and space fixed eckart frame.

	rlx	Δvar.	P_{trans}	c_{harm}^2	μ_x^{ii}	μ_z^{ii}	μ_x^{0i}	μ_z^{0i}	S	S_z
	[cm^{-1}]	[cm^{-1}]			[a.u.]	[a.u.]	[a.u.]	[a.u.]	$[\frac{km}{mol}]$	$[\frac{km}{mol}]$
000000	0.0	0.00	1.0000	0.910	0.738	-0.271	0.7384	-0.2711	-	-
000010	600.9	0.38	1.0000	0.749	0.720	-0.228	0.0438	-0.1096	135.4	233.6
000100	796.0	0.30	1.0000	0.694	0.723	-0.237	-0.0384	0.0932	131.0	224.0
000002	1055.4	-0.91	1.0000	0.878	0.676	-0.222	-0.0142	-0.0031	3.6	0.3
000020	1188.1	0.49	1.0000	0.563	0.701	-0.183	0.0030	-0.0091	1.8	3.2
001000	1267.6	-0.86	1.0000	0.771	0.724	-0.259	-0.0159	0.0901	171.9	333.5
000110	1385.3	0.45	1.0000	0.512	0.705	-0.194	-0.0064	0.0113	3.8	5.7
000200	1574.8	0.32	1.0000	0.442	0.710	-0.206	-0.0054	0.0036	1.1	0.7
000012	1640.9	-0.71	1.0000	0.688	0.655	-0.173	-0.0012	0.0004	0.0	0.0
010000	1690.0	-8.19	1.0000	0.799	0.750	-0.292	0.0510	-0.0575	161.8	181.1
000030	1761.6	0.22	1.0000	0.373	0.682	-0.137	-0.0007	0.0001	0.0	0.0
000102	1829.0	-0.78	1.0000	0.592	0.657	-0.188	-0.0003	0.0008	0.0	0.0
001010	1858.4	-1.04	1.0000	0.531	0.705	-0.213	0.0044	0.0010	0.6	0.1
000120	1961.6	0.18	1.0000	0.305	0.687	-0.150	-0.0011	0.0017	0.1	0.2
000004	2025.4	-1.71	1.0000	0.790	0.608	-0.168	0.0003	-0.0001	0.0	0.0
001100	2049.0	-0.86	1.0000	0.443	0.709	-0.224	0.0021	-0.0031	0.5	0.6
000210	2153.9	0.21	1.0000	0.247	0.691	-0.164	0.0014	-0.0019	0.2	0.3
000022	2210.7	-0.95	1.0000	0.469	0.633	-0.122	0.0001	-0.0002	0.0	0.0
010010	2291.1	-8.29	1.0000	0.584	0.732	-0.250	-0.0024	0.0057	1.4	2.4
001002	2306.5	-3.17	1.0000	0.743	0.658	-0.205	0.0006	-0.0007	0.0	0.0
000040	2321.8	-0.98	1.0000	0.207	0.663	-0.091	0.0002	-0.0006	0.0	0.0
000300	2339.4	0.11	1.0000	0.224	0.696	-0.178	-0.0010	0.0018	0.2	0.2
000112	2401.4	-1.36	1.0000	0.358	0.635	-0.138	0.0001	-0.0001	0.0	0.0
001020	2434.8	-2.67	1.0000	0.312	0.685	-0.165	0.0000	0.0008	0.0	0.1

37

TABLE VII: Following of Table VI.

rlx	Δvar.	P_{trans}	c^2_{harm}	μ^{ii}_x	μ^{ii}_z	μ^{0i}_x	μ^{0i}_z	S	S_z
	[cm^{-1}]	[cm^{-1}]			[a.u.]	[a.u.]	[a.u.]	[a.u.]	[$\frac{km}{mol}$]	[$\frac{km}{mol}$]
010100	2484.5	-7.97	1.0000	0.543	0.733	-0.254	0.0031	-0.0057	1.7	2.6
002000	2513.0	-4.48	1.0000	0.638	0.710	-0.244	-0.0066	0.0028	2.1	0.7
000130	2525.0	-1.33	1.0000	0.112	0.668	-0.105	-0.0002	0.0005	0.0	0.0
000202	2583.8	-1.87	0.9998	0.201	0.612	-0.137	0.0001	-0.0002	0.0	0.0
000014	2594.1	-1.96	1.0000	0.475	0.607	-0.131	0.0000	0.0001	0.0	0.0
001110	2627.7	-2.96	1.0000	0.235	0.689	-0.178	0.0003	-0.0012	0.1	0.1
000220	2720.5	-1.32	1.0000	0.049	0.672	-0.119	0.0002	-0.0002	0.0	0.0
010002	2729.9	-9.16	1.0000	0.737	0.677	-0.232	-0.0005	0.0007	0.0	0.1
000104	2758.9	-3.97	0.9994	0.290	0.576	-0.136	0.0001	-0.0002	0.0	0.0
000032	2764.9	-2.36	1.0000	0.255	0.610	-0.071	0.0001	-0.0001	0.0	0.0
001200	2813.9	-1.96	1.0000	0.163	0.694	-0.193	0.0007	-0.0010	0.1	0.1
000050	2866.4	-4.50	1.0000	0.041	0.652	-0.066	0.0002	-0.0001	0.0	0.0
001012	2878.8	-5.94	1.0000	0.474	0.635	-0.152	0.0000	-0.0001	0.0	0.0
010020	2881.0	-8.90	1.0000	0.394	0.705	-0.188	-0.0002	0.0004	0.0	0.0
000006	2905.9	-3.30	0.9936	0.539	0.537	-0.115	0.0000	0.0000	0.0	0.0
000310	2909.1	-1.58	1.0000	0.047	0.677	-0.135	-0.0001	0.0000	0.0	0.0
011000	2948.1	-10.58	1.0000	0.687	0.737	-0.280	-0.0006	0.0026	0.3	0.6
000122	2958.6	-3.44	1.0000	0.127	0.611	-0.087	0.0000	0.0000	0.0	0.0
001030	2997.3	-8.08	0.9989	0.139	0.664	-0.118	0.0000	0.0002	0.0	0.0
001102	3063.8	-5.82	1.0000	0.355	0.638	-0.171	0.0000	0.0001	0.0	0.0
010110	3070.9	-7.17	1.0000	0.321	0.701	-0.182	-0.0001	0.0003	0.0	0.0
000140	3077.1	-5.80	1.0000	0.021	0.664	-0.097	0.0001	-0.0002	0.0	0.0
000400	3091.1	-2.85	1.0000	0.074	0.685	-0.167	0.0002	0.0002	0.0	0.0
002010	3093.6	-9.88	1.0000	0.308	0.690	-0.184	-0.0004	-0.0001	0.0	0.0
000024	3131.0	-5.77	0.9849	0.202	0.535	-0.073	0.0001	-0.0001	0.0	0.0
000212	3151.9	-4.54	0.9999	0.107	0.605	-0.096	0.0000	-0.0001	0.0	0.0
001120	3193.1	-10.94	1.0000	0.056	0.669	-0.132	0.0000	0.0002	0.0	0.0
001004	3251.7	-6.70	0.9994	0.647	0.582	-0.144	0.0000	0.0000	0.0	0.0
010200	3257.6	-9.00	1.0000	0.318	0.717	-0.223	0.0010	-0.0018	0.2	0.4
000230	3274.5	-7.30	0.9998	0.099	0.652	-0.075	0.0001	-0.0001	0.0	0.0
002100	3281.2	-8.10	0.9872	0.236	0.675	-0.215	-0.0015	0.0009	0.2	0.1

TABLE VIII: Following of Tables VI and VII.

rlx	[cm⁻¹]	Δvar. [cm⁻¹]	P_{trans}	c^2_{harm}	μ_x^{ii} [a.u.]	μ_z^{ii} [a.u.]	μ_x^{0i} [a.u.]	μ_z^{0i} [a.u.]	S [$\frac{km}{mol}$]	S_z [$\frac{km}{mol}$]
000114	3292.3	-10.13	0.9305	0.048	0.431	-0.124	0.0001	-0.0001	0.0	0.0
000042	3303.6	-5.56	0.9992	0.073	0.586	-0.021	0.0001	-0.0001	0.0	0.0
010012	3319.9	-10.09	0.9961	0.534	0.646	-0.181	-0.0002	0.0002	0.0	0.0
000302	3336.6	-5.82	0.9998	0.132	0.617	-0.126	-0.0005	0.0007	0.0	0.1
020000	3349.6	-17.85	1.0000	0.657	0.760	-0.308	-0.0060	0.0086	6.0	8.1
001210	3381.9	-9.54	1.0000	0.001	0.674	-0.147	-0.0002	0.0003	0.0	0.0
000060	3401.8	-9.22	1.0000	0.007	0.624	0.003	0.0000	-0.0001	0.0	0.0
000008	3405.3	-14.38	0.8478	0.140	0.304	-0.112	-0.0004	0.0002	0.0	0.0
001022	3435.0	-13.57	0.9970	0.240	0.605	-0.099	0.0000	0.0000	0.0	0.0
010030	3454.2	-12.14	1.0000	0.236	0.690	-0.153	0.0001	-0.0002	0.0	0.0
000320	3467.2	-9.57	0.9997	0.093	0.659	-0.095	0.0000	0.0000	0.0	0.0
000016	3465.3	-12.16	0.9759	0.406	0.503	-0.085	0.0001	-0.0001	0.0	0.0
010102	3498.8	-9.80	0.9906	0.382	0.619	-0.165	0.0001	-0.0002	0.0	0.0
000132	3500.9	-9.77	0.9966	0.033	0.595	-0.065	-0.0001	0.0001	0.0	0.0
011010	3538.6	-12.76	1.0000	0.395	0.709	-0.216	0.0000	0.0004	0.0	0.0
000204	3542.4	-10.50	0.8228	0.098	0.405	-0.141	0.0008	-0.0005	0.1	0.0
002002	3533.3	-27.89	0.9911	0.601	0.619	-0.184	-0.0004	0.0003	0.0	0.0
001040	3547.4	-18.50	0.9998	0.032	0.652	-0.087	0.0002	-0.0002	0.0	0.0
001300	3565.0	-7.69	0.9999	0.002	0.679	-0.165	0.0003	-0.0001	0.0	0.0
100000	3591.0	4.53	1.0000	0.841	0.749	-0.273	-0.0264	0.0181	59.5	38.2
000150	3614.0	-13.50	1.0000	0.119	0.630	-0.018	0.0002	-0.0001	0.0	0.0
010120	3644.5	-	0.9941	0.150	0.671	-0.142	0.0000	0.0000	0.0	0.0
000410	3654.0	-	0.9911	0.014	0.656	-0.132	0.0000	0.0000	0.0	0.0
000034	3658.6	-	0.8582	0.029	0.416	-0.072	-0.0002	0.0001	0.0	0.0
002020	3660.6	-	0.9985	0.156	0.674	-0.148	0.0001	-0.0001	0.0	0.0
010004	3681.9	-	0.7256	0.000	0.246	-0.319	-0.0004	0.0003	0.0	0.0
000222	3695.7	-	0.9616	0.001	0.548	-0.067	0.0000	0.0000	0.0	0.0
003000	3739.1	-	0.9998	0.476	0.701	-0.232	-0.0005	0.0007	0.0	0.1
001130	3745.5	-	0.9991	0.056	0.649	-0.087	0.0000	0.0000	0.0	0.0
000106	3747.7	-	0.6571	0.180	0.236	-0.168	0.0000	0.0000	0.0	0.0
001014	3793.4	-	0.8619	0.000	0.430	-0.141	-0.0003	0.0002	0.0	0.0

TABLE IX: Following of Tables VI, VII and VIII.

	rlx	Δvar.	P_{trans}	c^2_{harm}	μ^{ii}_x	μ^{ii}_z	μ^{0i}_x	μ^{0i}_z	S	S_z
	[cm^{-1}]	[cm^{-1}]			[a.u.]	[a.u.]	[a.u.]	[a.u.]	[$\frac{km}{mol}$]	[$\frac{km}{mol}$]
000124	3806.2	-	0.8108	0.035	0.370	-0.107	0.0000	0.0000	0.0	0.0
001202	3811.5	-	0.9846	0.000	0.565	-0.118	0.0000	0.0000	0.0	0.0
000240	3815.8	-	0.9999	0.166	0.627	-0.025	0.0000	0.0000	0.0	0.0
010210	3826.3	-	0.9912	0.079	0.667	-0.144	0.0001	-0.0001	0.0	0.0
000052	3828.9	-	1.0000	0.028	0.575	0.019	0.0000	0.0000	0.0	0.0
000500	3838.3	-	0.9986	0.030	0.680	-0.158	0.0001	-0.0002	0.0	0.0
002110	3851.0	-	0.9971	0.099	0.679	-0.168	0.0000	0.0001	0.0	0.0
000312	3883.4	-	0.7561	0.001	0.383	-0.220	0.0000	0.0000	0.0	0.0
010022	3893.7	-	0.6394	0.001	0.288	-0.163	-0.0002	0.0001	0.0	0.0
000070	3923.9	-	0.9998	0.024	0.604	0.050	0.0000	0.0000	0.0	0.0
001220	3936.6	-	0.9973	0.105	0.652	-0.105	0.0001	-0.0002	0.0	0.0
000026	3991.4	-	0.7774	0.173	0.333	-0.096	0.0000	0.0000	0.0	0.0

TABLE X: Comparison of calculated and experimental transition energies in cm^{-1} at the *trans* geometry. Given in parentheses are the transition moments in km/mol.

	ν_{exp} [a]	Calc.[b]	Calc.[c]	Calc. [d]	Calc. [e]	var. [f]	CCSD(T)/DFT [g]
000010	596	590(139)	549(175)	580(186)	602(182)	600.5	600.9(135)
000100	790(139)	796(128)	763(133)	804(44)	796(143)	795.7	796.0(131)
001000	1263	1308(169)	1217(216)	1245(550)	1260(179)	1268.5	1267.6(172)
010000	1700	1696 (129)	1620(143)	1764(116)	1653(94)	1698.2	1690.0(162)
100000	3591	3785(76)	3560(122)	3596(35)	3587(83)	3586.5	3591.0(60)
000002	-	-	890(37)	1080(5)	1093(6)	1056.3	1055.4(4)

[a]From Ref. [6]
[b]CCSD(T) calculations from Ref. [66].
[c](MP2/CC-VSCF)/HF 2D-anharmonic calculations from Ref. [3].
[d]DFT, 6D-anharmonic calculations from [60].
[e]MP2/3D-anharmonic from [62].
[f]From [21].
[g]This work.

TABLE XI: Comparison of the different values of k from eq. (15) in the text and the final trans probability P_{trans}^F for different total energies and laser intensities. The laser frequency is equal to 850 cm^{-1}.

laser intensity [a.u.]	total Energy [eV]	k [ps^{-1}]	P_{trans}^F (t=2500 fs)
0.0035	1.045	0.67	0.17
0.004	1.128	0.89	0.22
0.005	1.260	1.80	0.28
0.006	1.363	2.66	0.34

FIG. 1: Definition of the six valence polyspherical coordinates.
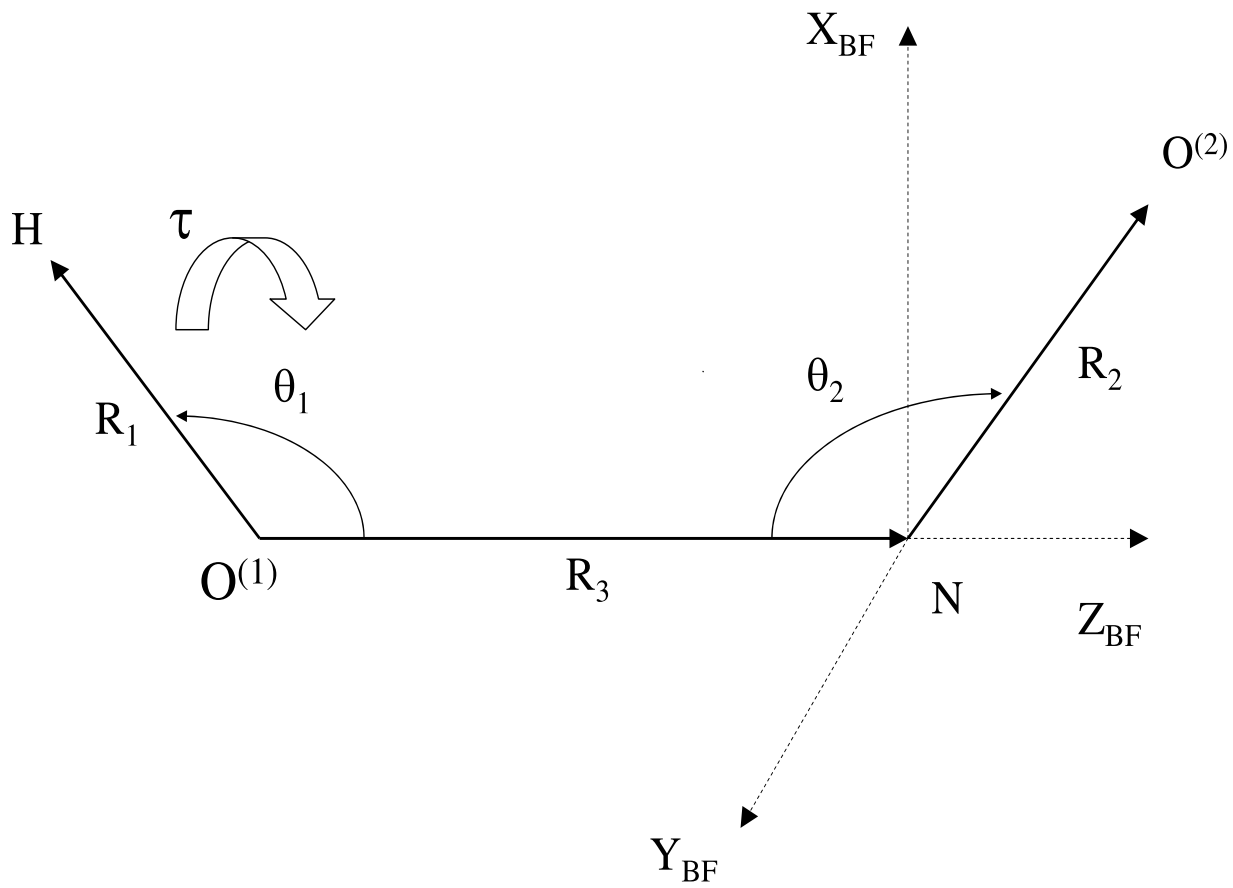
FIG. 2: Reduced (i.e. integrated over the other degrees of freedom) density plots of calculated eigenfunctions as labeled at the left upper corner in the R_3, $\cos(\theta_2)$ plane. The right column shows the ν_4 overtone series 000a00 (a=2,3,4,5) and the plots in the left column at the same row present present the 0100(a-2)0 counterpart of the resonant pair (0100(a-2)0/000a00). The dashed line in each picture represents the path where B_τ is minimal with respect to the total potential energy.
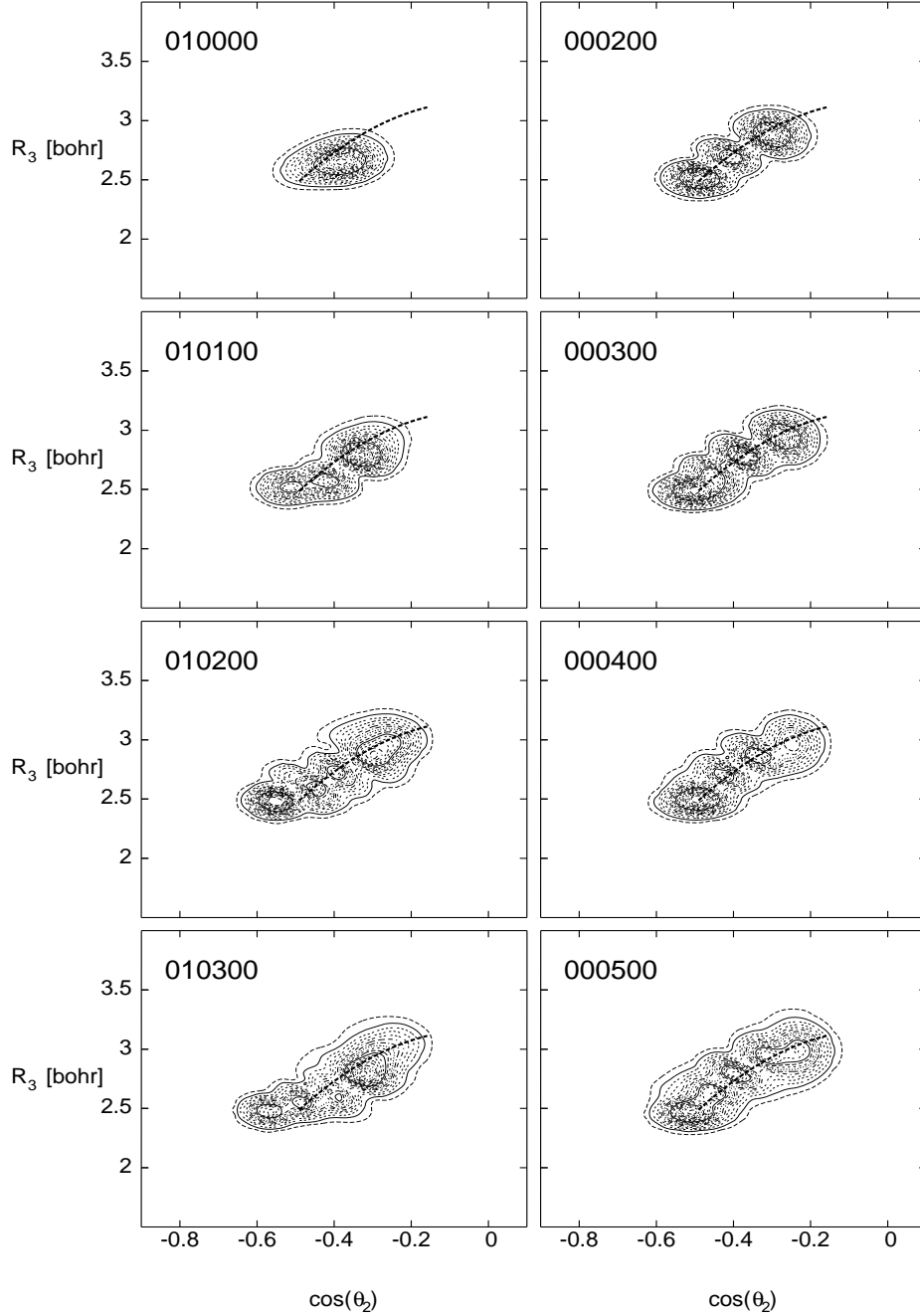
FIG. 3: Z-components of the transition moments (e a_o): $t_{ij} = |< \Psi_i|\hat{\mu}_z|\Psi_j >|$ in terms of E_j and $\Delta E_{ij} = E_j - E_i$. E_i (E_j) is the eigenvalue associated with the eigenvector Ψ_i (Ψ_j) and $E_j > E_i$.
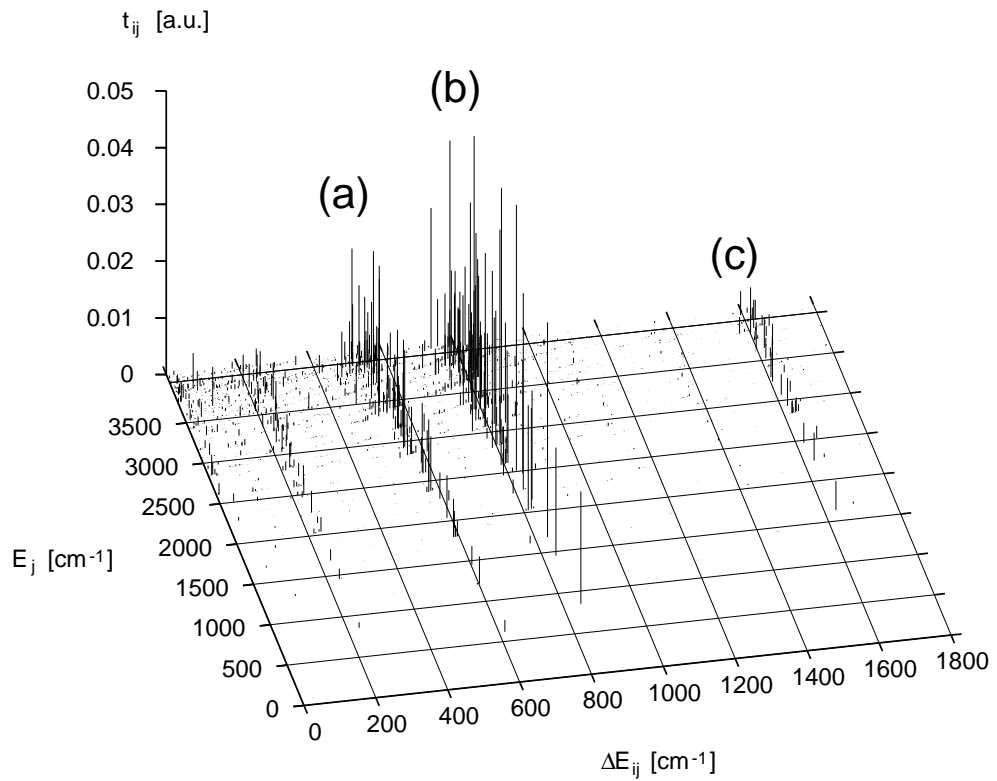
FIG. 4: In solid line, the squared overlap between the wavepacket after excitation by means of the laser light defined in Section VI and all the converged eigenstates. In dashed line, the Fourier transform of the autocorrelation function (arbitrary unit).
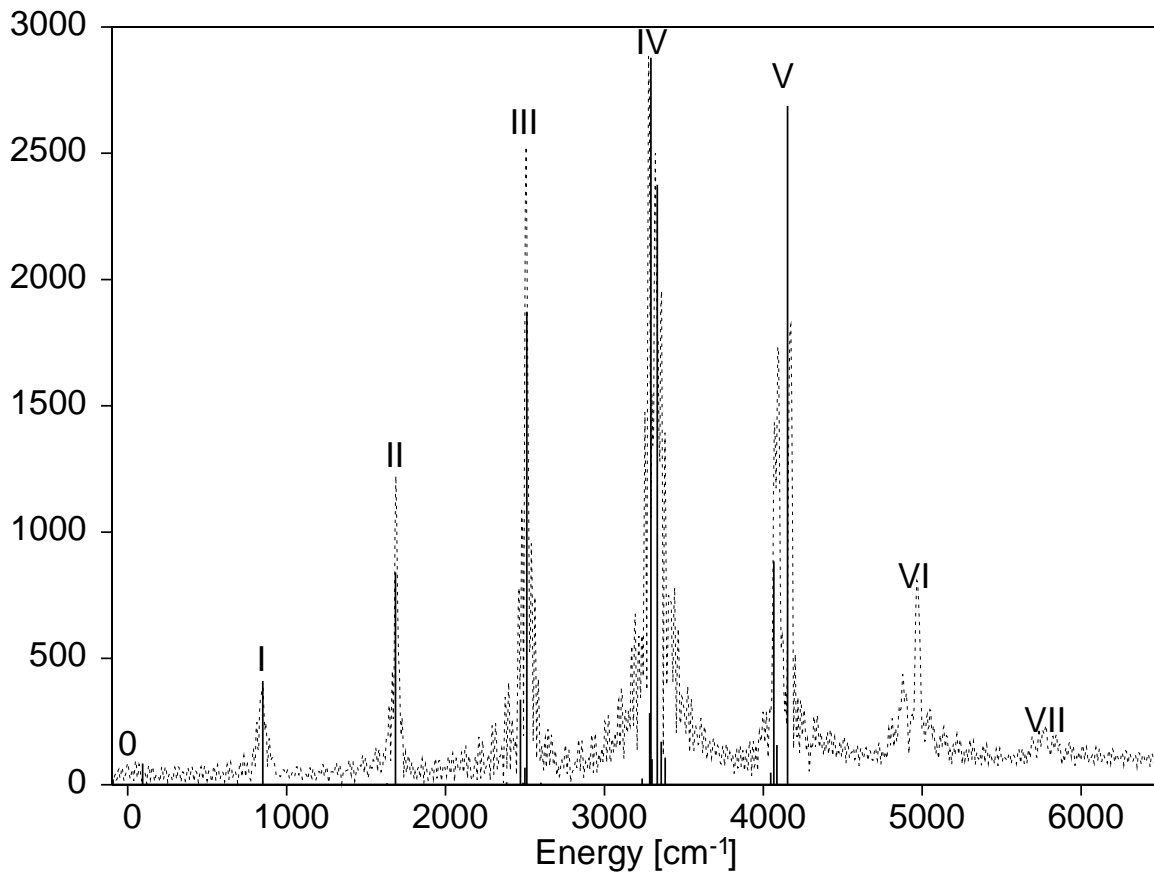
FIG. 5: Evolution of the population of the groups corresponding to the Figure 4. The values for 0, I, II, III, IV, V were obtained by summation of the population over all levels within the energy ranges 0-250, 700-950, 1500-1750, 2250-2750, 3250-3500, 400-4250 cm^{-1} respectively. The parameters of the pulse are $\omega = 850$ cm^{-1} and E$_o = 0.0035$ a.u.
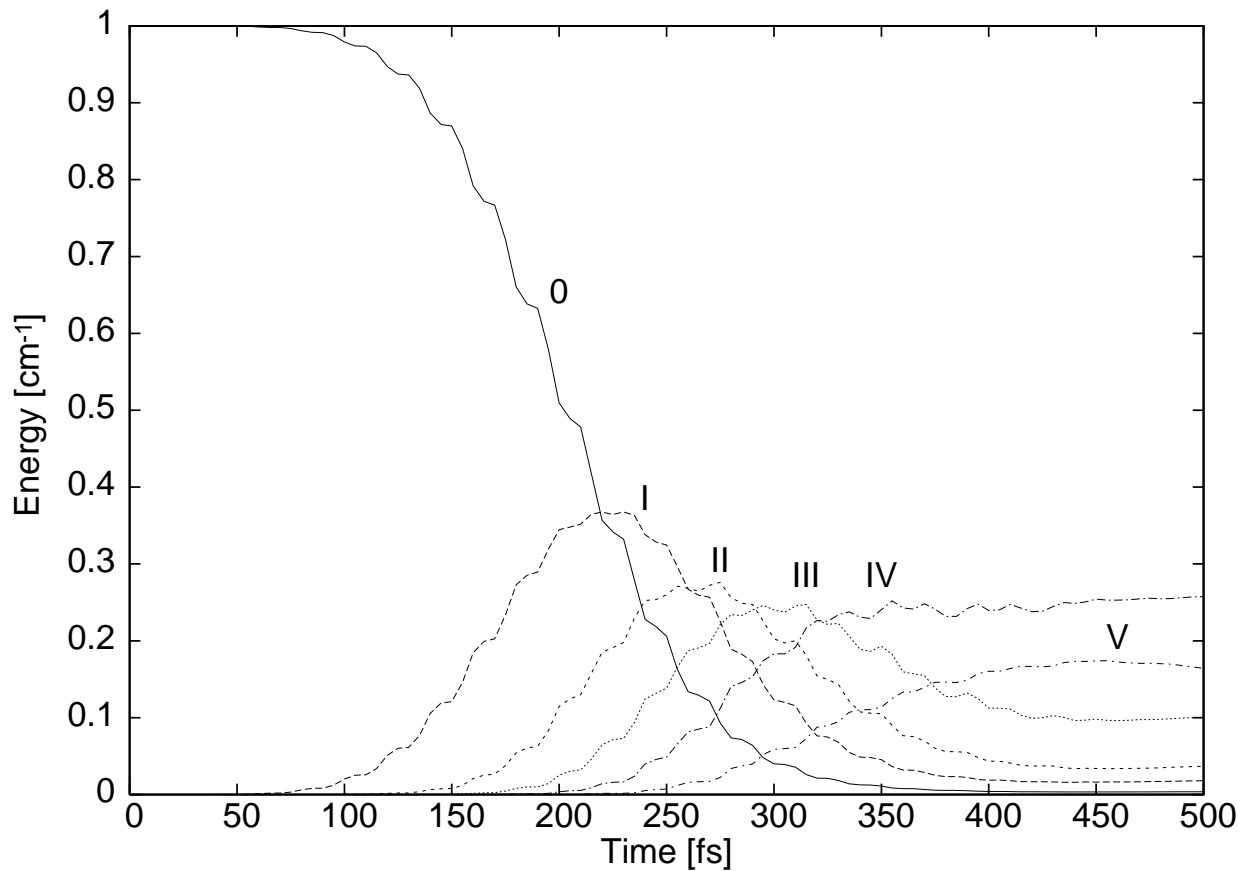
FIG. 6: Time evolution of the meanvalues of ON, or R_3, (thick broken lines, upper picture), ONO, or θ_2 (thin broken lines, upper picture), N=O, or R_2, (thick broken lines lower picture), and HON, or θ_1, (thin broken lines, lower picture) and of P_{trans} (solid line, upper picture) during the excitation ($E_0 = 0.0035 a.u.$). The Y-axis gives the value of P_{trans}. The stretches are scaled like $< R > = (< R > (t) - < R >_0) / < R >_0 / f$ and the angles like $< \cos\theta > = (< \cos\theta > (t) - < \cos\theta >_0)$. $< R >_0$ and $< \theta >_0$ denote the grounstate averaged values and $f = 10$.
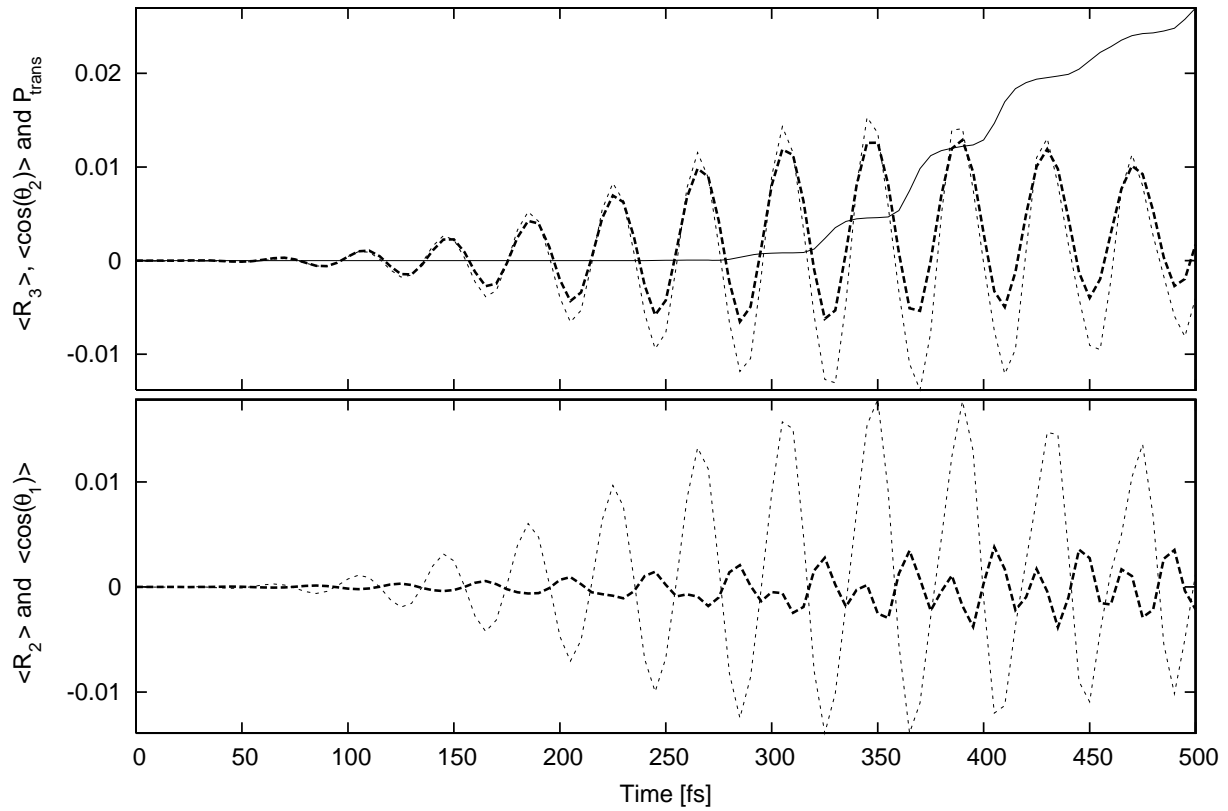
FIG. 7: Reduced density logarithmic contourplots of the wavepacket in the R_3, τ plane during the laser excitation using a carrier frequency corresponding to 850 cm^{-1}, a maximal field strength of 0.0035 a.u. and a $\sin^2$ pulse-envelope with a duration of 500 fs. Underlayed is the PES with the other coordinates fixed at cis eqilibrium.
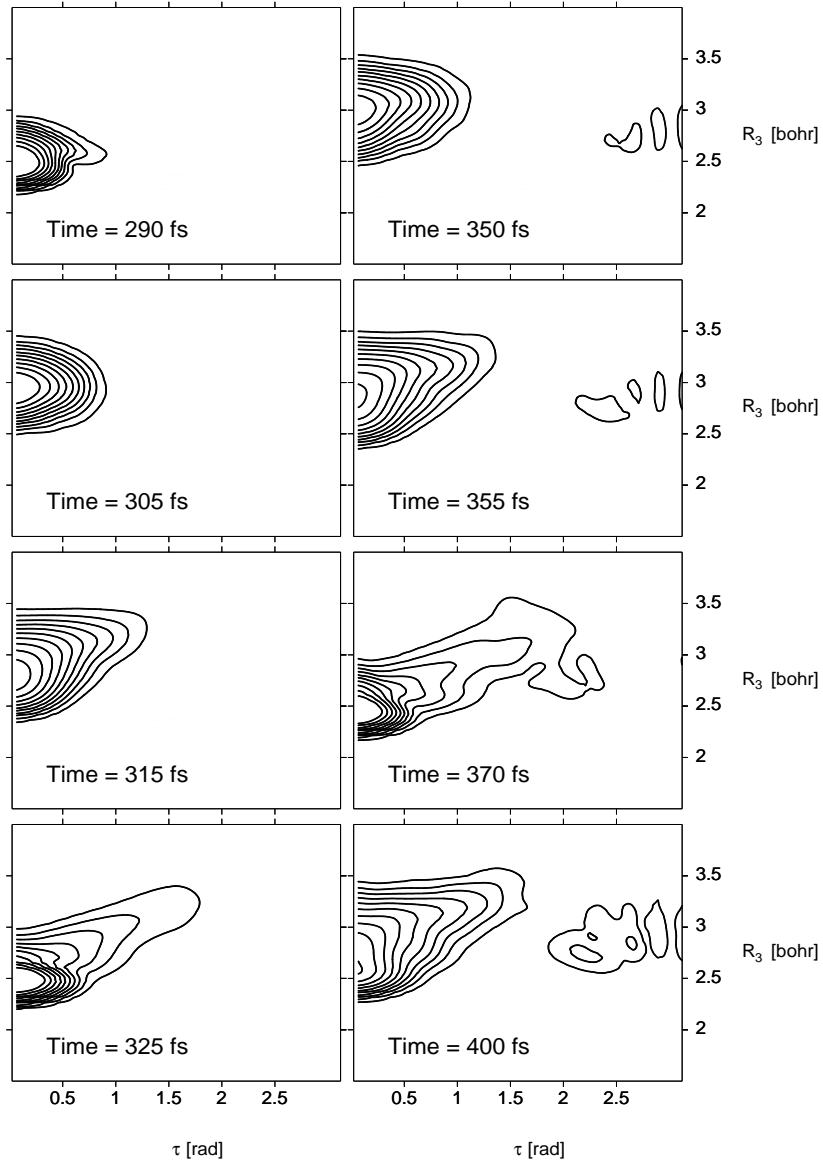
FIG. 8: Time evolution of the scaled meanvalues of ON, or R_3, (thick broken lines) and ONO, or θ_2, (thin broken lines) and of P_{trans} (solid line). The Y-axis gives the value of P_{trans}. The other meanvalues are scaled like in Figure 6 with $f = 1$.
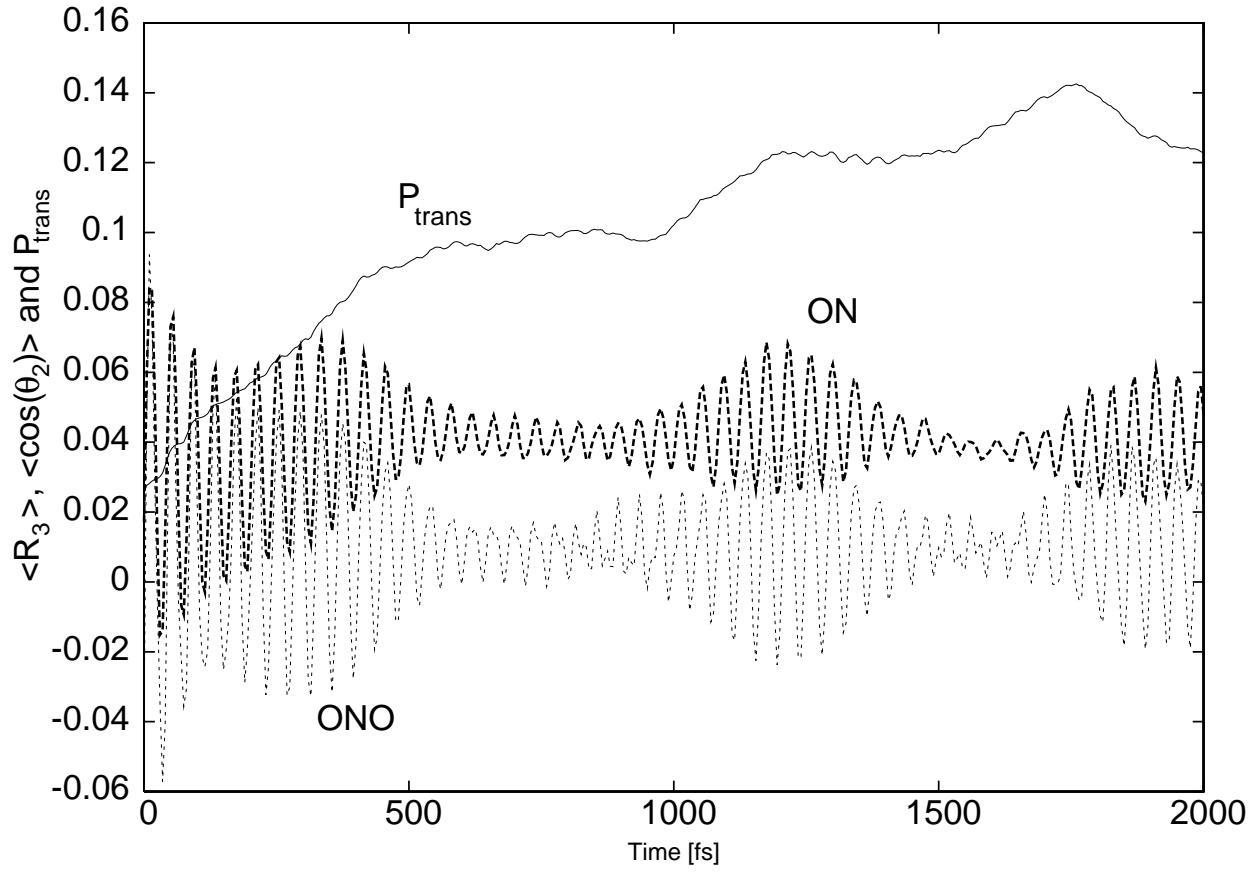
FIG. 9: Time evolution of the energies in the harmonic modes. ω_2 to the N=O stretch, ω_3 to the HON bend, ω_4 to the 'asymetric' mixture of $Q^-_{ONO/ON}$, ω_5 to the 'symetric' mixture of $Q^+_{ONO/ON}$, and ω_6 to the torsion.

50